Supplemental Information for
Significant temperature dependence of the isosteric heats of adsorption of gases in zeolites demonstrated by experiments and molecular simulations

Alexander S. Hyla,[1†] Hanjun Fang,[1] Salah Eddine Boulfelfel,[1] Giovanni Muraro,[2] Charanjit Paur,[2] Karl Strohmaier,[2] Peter I. Ravikovitch,[2]* David S. Sholl[1]*

[1] School of Chemical & Biomolecular Engineering, Georgia Institute of Technology, Atlanta, GA 30332-0100, USA.

[2] Corporate Strategic Research, ExxonMobil Research and Engineering, 1545 Route 22 East, Annandale, NJ 08801, USA

† Current Address: Department of Chemical & Petroleum Engineering, University of Calgary, 2500 University Dr. NW, Calgary, AB T2N 1N4, Canada

* Corresponding authors e-mails: peter.ravikovitch@exxonmobil.com, david.sholl@chbe.gatech.edu

Choice of force field for study:

11 different force fields in the literature were found to have parameters that describe the adsorption of CO_2 in siliceous zeolites.[1-11] For each of the force fields, if an adsorbate-adsorbate model was given (EPM2[12] or TraPPE[13]), that was used for the GCMC simulations describing the adsorption of CO_2 in ITQ-29 at 195 K, as described in the main paper. The simulated adsorption isotherms are presented below in Figure S1, along with 2 experimental isotherms obtained from calorimetric measurements from this work. The CCFF results are by far the closest to the experimental results. All but 3 of the force fields examined predict the same general shape of the isotherm as the isotherms obtained from the calorimetric measurements, but deviate from the experimental isotherms in the region around 1,000 Pa. The CCFF results show almost quantitative agreement with the experiments. This region of the isotherm is where the loadings start to increase towards saturation loading. Since the simulations are performed at the same pressures, a direct comparison of the force fields to CCFF results can be performed and the results are shown below in Figure S2. The parameters of all 11 force fields used in this study can be found in Table S2.

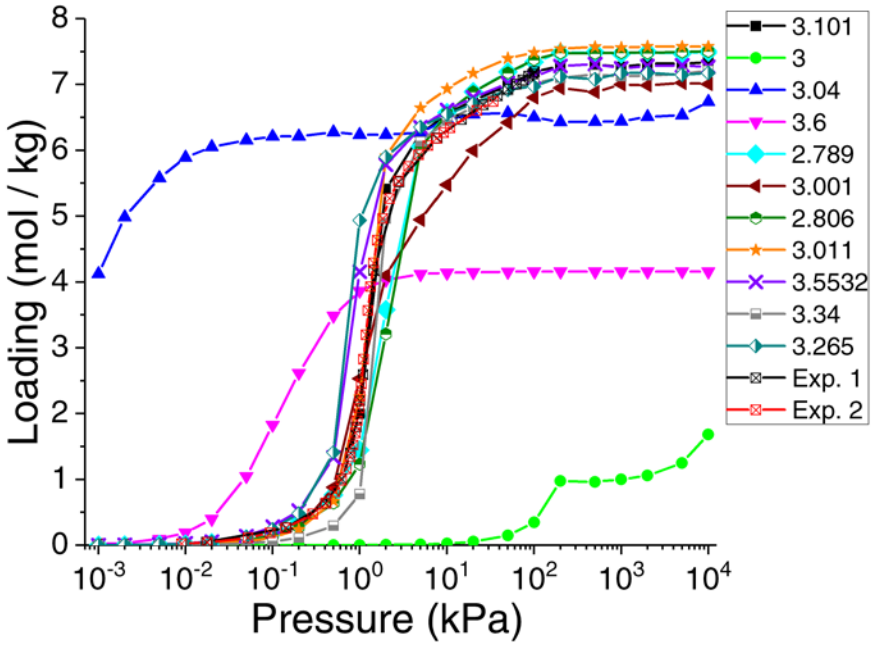

Figure S1: Comparison of adsorption isotherms calculated by 11 different force fields for CO_2 in ITQ-29 at 195 K to two experimental calorimetric measurements from this work. The results are labeled by the σ parameter from the force field for the oxygen atoms in the zeolite framework. The data labeled 3.101 is our CCFF results.

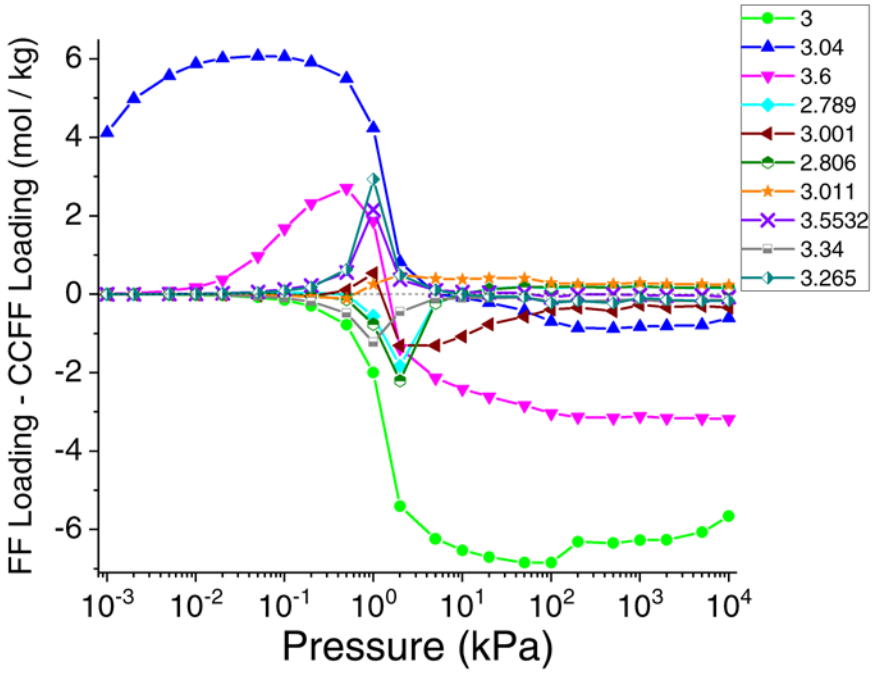

Figure S2: Comparison of the loadings calculated by the literature force fields versus the CCFF results. The results are labeled by the σ parameter from the force field for the oxygen atoms in the zeolite framework. The dotted line is the CCFF results. The region around 1,000 Pa corresponds to the region of the isotherm where the loading starts to rapidly increase towards the saturation loading.

Force Field Development for CH_4 in Na-exchanged Zeolites

Recently, we implemented an approach to developing first-principles-based force fields for CH_4 in siliceous zeolites.[14] This approach uses the fully periodic framework to represent the adsorbent structure and relies on electronic structure calculations for hundreds or thousands of adsorption configurations scattered throughout the framework. Both united-atom (UA) and all-atom (AA) models were tested for CH_4 in siliceous zeolites, and they performed similarly well in predicting adsorption and diffusion properties. Here we extend our approach to Na-exchanged zeolites, where Na-LTA with Si/Al = 3 ($Na_6Al_6Si_{18}O_{48}$) is used as the zeolite model and the AA CH_4 model is chosen considering the stronger Coulomb interactions for CH_4 in cationic zeolites than in siliceous zeolites. The details about the force field potential can be found in our previous work.[14]

Similar to siliceous zeolites, DFT/CC (density functional theory/coupled cluster) method is used to get reliable interaction energies of CH_4 in the Na-exchanged zeolite model.[14, 15] The CC correction functions for Si, and O are taken from our previous calculations for siliceous zeolites,[14] and for Al they are treated the same as Si. The CC correction functions for Na cations are not considered as discussed by Otero Arean et al.[16] The configurations in force field fitting data sets are from conventional NVT (N = 1, T = 300 K) Monte Carlo simulations, where the force field parameters for AA CH_4 interacting with Si and O are retained for Na-exchanged zeolites. In the first iteration, the ClayFF parameters[9] are used for Al and Na, TraPPE parameters[17] for the C atom of CH_4, and DDEC3 charges[18-20] for the atoms of CH_4. Lorentz-Berthelot mixing rules are applied for the Lennard-Jones for cross interacting species. A total of 1000 configurations are chosen from the NVT MC snapshots and used in force field fitting. The fitted FF parameters are then used in the next iteration following the same procedure. We perform this procedure for several iterations until the vdW (van der Waals) force field parameters for the atoms of CH_4 and zeolite (Al and Na) are converged (the changes of the parameters are within ± 3 %). The resulting force field (denoted CCFF) parameters for CH_4 in Na-containing zeolites are summarized in Table S1.

A detailed comparison of the interaction energies predicted with CCFF and the corresponding energies at the DFT/CC level is shown in Figure S3. The DFT/CC calculations of the last iteration span a range of adsorption energies, from -21 to -1 kJ/mol. As expected from their derivation, the CCFF interaction energies are reasonably consistent with the DFT/CC results. The residual standard deviation (RSD) and mean deviation (MD) between the force field and the DFT/CC results are 1.4 and 0.1 kJ/mol, respectively.

We validated CCFF by comparing the simulated adsorption isotherms and isosteric heats of adsorption for CH_4 in LTA-4A and Na-LTA (Si/Al = 2 and 5) with available experimental data. In these simulations, the force field parameters for cation–framework interactions are from our previous work of CO_2 adsorption in Na- exchanged zeolites.[1] The validation results are shown in Figure S4. CCFF performs reasonably well for CH_4 adsorption in these three Na-exchanged zeolites. The parameters of the force fields used in this study can be found in Tables S2 and S3.

Table S1: Force field parameters for all-atom (AA) CH_4 in Na-exchanged zeolites, derived from DFT/CC calculations in this work. This force field is defined as CCFF.

Cross species	CCFF		
	ε/k_B (K)	σ (Å)	Atomic charge (e)
AA CH_4 (C_CH_4 and H_CH_4)			
Si_{zeo}–C_CH_4	33.98[a]	3.845[a]	Si_{zeo} (2.2124)[a]
Si_{zeo} –H_CH_4	24.15[a]	3.298[a]	O_{zeo}^{Si} (-1.1062)[a]
O_{zeo}–C_CH_4	19.88[a]	3.391[a]	O_{zeo}^{Al} (-1.3211)
O_{zeo}–H_CH_4	16.17[a]	2.844[a]	Al_{zeo} (2.0833)
Al_{zeo}–C_CH_4	42.83	3.460	Na_{zeo} (0.9887)
Al_{zeo}–H_CH_4	31.21	2.956	C_CH_4 (-0.516)[a]
Na_{zeo}–C_CH_4	88.79	2.906	H_CH_4 (0.129)[a]
Na_{zeo}–H_CH_4	78.92	2.401	

[a] The parameters from our previous work of AA CH_4 in siliceous zeolites are retained for Na-exchanged zeolites.[14]

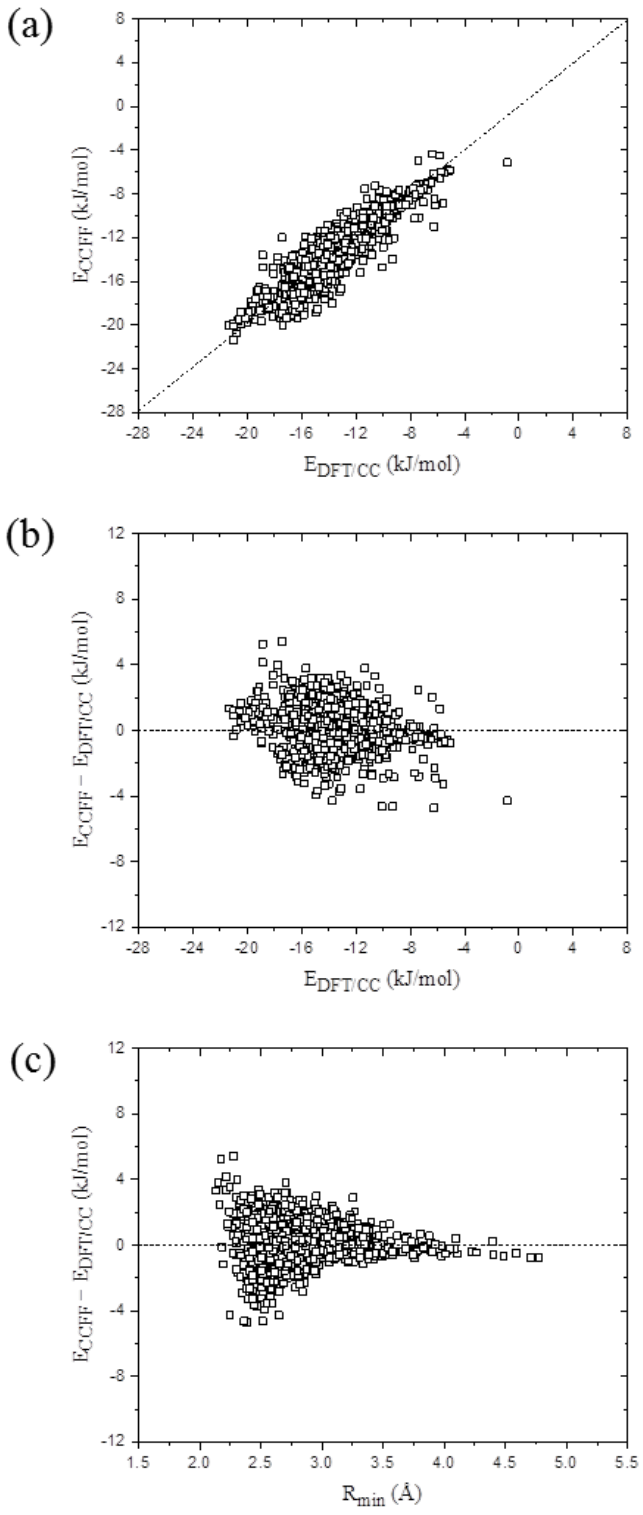

Figure S3: Force field fitting results of the last iteration for CH_4 in Na-LTA (Si/Al = 3): (a) comparison of the interaction energies of CH_4 in zeolite for CCFF and DFT/CC, (b) the difference in interaction energies, $E_{CCFF} - E_{DFT/CC}$, as a function of $E_{DFT/CC}$, and (c) $E_{CCFF} - E_{DFT/CC}$ as a function of the minimum atomic distance between CH_4 and zeolite. A total of 1000 CH_4 configurations are included.

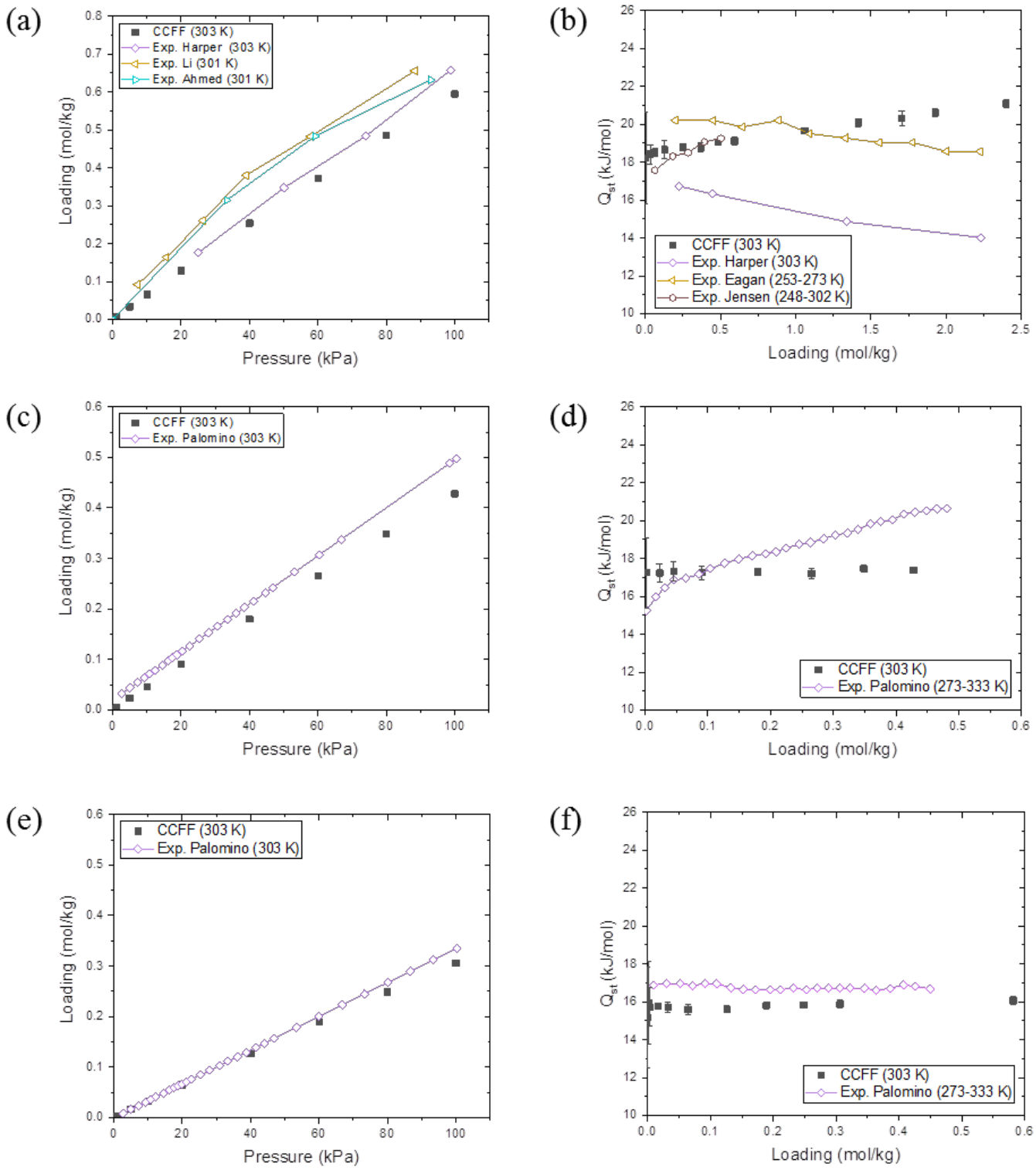

Figure S4: Comparison of simulated (CCFF) and experimental adsorption isotherms and heats of adsorption of CH_4 in (a and b) LTA-4A, (c and d) Na-LTA with Si/Al = 2, and (e and f) Na-LTA with Si/Al = 5. The experimental data are from Harper et al.,[21] Li et al.,[22] Ahmed et al.,[23] Eagan et al.,[24] Jensen et al.,[25] and Palomino et al.[26]

Table S2: Force field parameters for siliceous zeolites used in this study. ε/k_B has units of K, σ has units of Å, masses are given in atomic mass units (amu), and charges are given in amu.

Force Field	**CCFF**[a] σ = 3.101	σ = 3	σ = 3.04	σ = 3.6	σ = 2.789	σ = 3.001	σ = 2.806	σ = 3.011	σ = 3.5532	σ = 3.34	σ = 3.265
						CO_2					
CO_2 model	EPM2	EPM2	TraPPE	EPM2	TraPPE	EPM2	EPM2	EPM2	EPM2	TraPPE	TraPPE
Interaction Model	Lennard-Jones	Lennard-Jones	Lennard-Jones	Lennard-Jones	Lennard-Jones	Lennard-Jones	Lennard-Jones	Lennard-Jones	Lennard-Jones	Lennard-Jones	Lennard-Jones
Mixing rules	Lorentz-Berthelot	Lorentz-Berthelot	Lorentz-Berthelot	Lorentz-Berthelot	Lorentz-Berthelot	Lorentz-Berthelot	Lorentz-Berthelot	Lorentz-Berthelot	Lorentz-Berthelot	Lorentz-Berthelot	Lorentz-Berthelot
$C_{CO2} - O_{zeo}$	ε = 29.116 σ = 3.193	ε = 24.372 σ = 2.9	ε = 61.41 σ = 2.897	ε = 42.125 σ = 3.9	ε = 50.20 σ = 2.7815	ε = 37.595 σ = 3.511	ε = 29.116 σ = 3.193	ε = 38.24537 σ = 2.884	ε = 46.90 σ = 2.96	ε = 37.82856 σ = 3.050	ε = 44.15201 σ = 3.050
$C_{CO2} - Si_{zeo}$	ε = 49.754 σ = 3.620	None	None	None	None	None	ε = 49.754 σ = 3.620	ε = 29.99276 σ = 2.8635	ε = 0.16 σ = 3.03	ε = 24.37212 σ = 2.550	None
$O_{CO2} - O_{zeo}$	ε = 23.433 σ = 3.067	ε = 41.689 σ = 3.025	ε = 118.793 σ = 3.255	ε = 69.743 σ = 3.48	ε = 84.93 σ = 2.9195	ε = 78.98 σ = 3.237	ε = 23.433 σ = 3.067	ε = 64.70212 σ = 3.022	ε = 79.35 σ = 3.10	ε = 64.70703 σ = 3.175	ε = 75.52351 σ = 3.1575
$O_{CO2} - Si_{zeo}$	ε = 38.900 σ = 3.494	None	None	None	None	None	ε = 38.900 σ = 3.494	ε = 50.74065 σ = 3.0015	ε = 0.27 σ = 3.17	ε = 41.68933 σ = 2.675	None
$C_{CO2} - C_{CO2}$	ε = 28.129 σ = 2.757	ε = 27.000 σ = 2.8	ε = 29.125 σ = 2.753	ε = 46.650 σ = 3.83	ε = 28.129 σ = 2.76	ε = 29.933 σ = 2.745	ε = 28.129 σ = 2.757	ε = 28.129 σ = 2.757	ε = 28.129 σ = 2.757	ε = 27.000 σ = 2.8	ε = 27.000 σ = 2.8
$O_{CO2} - O_{CO2}$	ε = 80.507 σ = 3.033	ε = 79.000 σ = 3.05	ε = 110.236 σ = 3.47	ε = 76.474 σ = 3.36	ε = 80.507 σ = 3.033	ε = 85.671 σ = 3.017	ε = 80.507 σ = 3.033	ε = 80.507 σ = 3.033	ε = 80.507 σ = 3.033	ε = 79.000 σ = 3.05	ε = 79.000 σ = 3.05
$C_{CO2} - O_{CO2}$	None	ε = 46.184 σ = 2.925	ε = 56.88 σ = 3.112	ε = 18.335 σ = 3.31	ε = 47.59 σ = 2.89	ε = 50.64 σ = 2.88	None	ε = 47.58762 σ = 2.895	ε = 47.58762 σ = 2.895	ε = 46.18441 σ = 2.925	ε = 46.18441 σ = 2.925
						Atom properties					
C_{CO2} mass (charge)	12.0 (0.6512)	12.0 (0.7000)	12.0 (0.8000)	12.0 (0.7200)	12.0 (0.6512)	12.0 (0.65)	12.0 (0.6512)	12.0 (0.6512)	12.0 (0.6512)	12.0 (0.7000)	12.0 (0.7000)
O_{CO2} mass (charge)	15.9994 (-0.3256)	15.9994 (-0.3500)	15.9994 (-0.4000)	15.9994 (-0.3600)	15.9994 (-0.3256)	15.9994 (-0.325)	15.9994 (-0.3256)	15.9994 (-0.3256)	15.9994 (-0.3256)	15.9994 (-0.3500)	15.9994 (-0.3500)
O_{zeo} mass (charge)	15.9994 (-1.1062)	15.9994 (-0.4000)	15.9994 (-1.8500)	15.9994 (-1.2000)	15.9994 (-1.0250)	15.9994 (-0.393)	15.9994 (-1.0000)	15.9994 (-0.7065)	15.9994 (-1.0500)	15.9994 (-0.7500)	15.9994 (-1.0000)
Si_{zeo} mass (charge)	28.0855 (2.2124)	28.0855 (0.8000)	28.0855 (3.7000)	28.0855 (2.4000)	28.0855 (2.0500)	28.0855 (0.786)	28.0855 (2.0000)	28.0855 (1.4130)	28.0855 (2.1000)	28.0855 (1.5000)	28.0855 (2.0000)
						CH_4 (CCFF only)[b]					
CH_4 model	TraPPE										
Mixing rules	Lorentz-Berthelot										
Interaction Model	Lennard-Jones										
CH_4_sp3 – O_{zeo}	ε = 109.759	σ = 3.416									
CH_4_sp3 – CH_4_sp3	ε = 148.0	σ = 3.73									
	Atom Properties										
	Mass	**Charge**									
CH_4	16.03176	0.0									
O_{zeo}	15.9994	-1.1062									
Si_{zeo}	28.0855	2.2124									
						N_2 (CCFF only)[c]					
N_2 model	2LJ3CB.MSKM potential										
Mixing rules	Lorentz-Berthelot										
Interaction Model	Lennard-Jones										
$N_2 - O_{zeo}$	ε = 27.31	σ = 3.14									
$N_2 - Si_{zeo}$	ε = 46.00	σ = 3.57									
$N_2 - N_2$	ε = 36.4	σ = 3.32									
	Mass	**Charge**									
N_2	14.0067	-0.40484									
N_2 C.O.M.	0	0.80968									
O_{zeo}	15.9994	-1.1062									
Si_{zeo}	28.0855	2.2124									

[a] Ref. 1; [b] Ref. 14; [c] Ref. 30;

Table S3: Force field parameters for cationic zeolites used in this study.

CCFF Force Field				
CO_2[a]				
CO_2 model	EPM2			
Mixing rules	Lorentz- Berthelot			
Force Field Parameters	**Interaction Model**	**ε/k_B (K)**	**σ (Å)**	
$C_{CO2} - O_{zeo}$	Lennard-Jones	29.116	3.193	
$C_{CO2} - Si_{zeo}$	Lennard-Jones	49.754	3.620	
$O_{CO2} - O_{zeo}$	Lennard-Jones	23.433	3.067	
$O_{CO2} - Si_{zeo}$	Lennard-Jones	38.900	3.494	
$C_{CO2} - Al_{zeo}$	Lennard-Jones	32.215	3.366	
$O_{CO2} - Al_{zeo}$	Lennard-Jones	25.323	3.246	
$C_{CO2} - Na_{zeo}$	Lennard-Jones	66.778	2.827	
$O_{CO2} - Na_{zeo}$	Lennard-Jones	54.762	2.707	
$C_{CO2} - C_{CO2}$	Lennard-Jones	28.129	2.757	
$O_{CO2} - O_{CO2}$	Lennard-Jones	80.507	3.033	
		A (K)	**B ($Å^{-1}$)**	**C (K)**
$Na_{zeo} - O_{zeo}$	Buckingham	37850656.24	3.8506	526402.05
Atom Properties				
	Mass (amu)	**Charge (amu)**		
C_{CO2}	12.0	0.6512		
O_{CO2}	15.9994	-0.3256		
O_{zeo}^{Si}	15.9994	-1.1062		
O_{zeo}^{Al}	15.9994	-1.3211		
Si_{zeo}	28.0855	2.2124		
Al_{zeo}	26.981539	2.0833		
Na_{zeo}	22.98977	0.9887		
CH_4[b]				
CH_4 model	TraPPE			
Mixing rules	Lorentz- Berthelot			
Force Field Parameters	**Interaction Model**	**ε/k_B (K)**	**σ (Å)**	
$C\_CH_4 - Si_{zeo}$	Lennard-Jones	33.979	3.845	
$H\_CH_4 - Si_{zeo}$	Lennard-Jones	24.151	3.298	
$C\_CH_4 - O_{zeo}$	Lennard-Jones	19.884	3.391	
$H\_CH_4 - O_{zeo}$	Lennard-Jones	16.173	2.844	
$C\_CH_4 - Al_{zeo}$	Lennard-Jones	42.834	3.460	
$H\_CH_4 - Al_{zeo}$	Lennard-Jones	31.210	2.956	
$C\_CH_4 - Na_{zeo}$	Lennard-Jones	88.789	2.906	
$H\_CH_4 - Na_{zeo}$	Lennard-Jones	78.916	2.401	
$C\_CH_4 - C\_CH_4$	Lennard-Jones	148.00	3.730	
		A (K)	**B ($Å^{-1}$)**	**C (K)**
$Na_{zeo} - O_{zeo}$	Buckingham2	37850656.24	3.8506	526402.05
Atom Properties				
	Mass (amu)	**Charge (amu)**		
C_CH_4	12.0	-0.516		
H_CH_4	1.00794	0.129		
O_{zeo}^{Si}	15.9994	-1.1062		
O_{zeo}^{Al}	15.9994	-1.3211		
Si_{zeo}	28.0855	2.2124		
Al_{zeo}	26.981539	2.0833		
Na_{zeo}	22.98977	0.9887		
N_2[c]				
N_2 model	2LJ3CB.MSKM potential			
Mixing rules	Lorentz- Berthelot			

Force Field Parameters	**Interaction Model**	**ε/k_B (K)**	**σ (Å)**	
$N_2 - O_{zeo}$	Lennard-Jones	27.31	3.14	
$N_2 - Si_{zeo}$	Lennard-Jones	46.00	3.57	
$N_2 - Al_{zeo}$	Lennard-Jones	39.51	3.71	
$N_2 - Na_{zeo}$	Lennard-Jones	82.64	2.659	
$N_2 - N_2$	Lennard-Jones	36.4	3.32	
		A (K)	**B ($Å^{-1}$)**	**C (K)**
$Na - O_{zeo}$	Buckingham2	37850656.24	3.8506	526402.05
Atom Properties				
	Mass (amu)	**Charge (amu)**		
N_2	14.0067	-0.40484		
N_2 C.O.M.	0	0.80968		
O_{zeo}^{Si}	15.9994	-1.1062		
O_{zeo}^{Al}	15.9994	-1.3211		
Si_{zeo}	28.0855	2.2124		
Al_{zeo}	26.981539	2.0833		
Na_{zeo}	22.98977	0.9887		

[a] Ref. 1; [b] Ref. 14 and this work; [c] Ref. 30;

Comparison of the ITQ-29 unit cell structure:

We performed simulations with the crystal structure from Corma,[31] as well as taking the average structure from molecular dynamics performed in the NPT ensemble, to allow for the volume and shape of the ITQ-29 structure to relax at the chosen temperature of 195 K. The same CCFF force field was used in the simulations for each structure. Comparison with experimental adsorption measurements from calorimetric measurements of ITQ-29 at 195 K from this work (Figure S5) confirms that both the crystal structure and the temperature dependent structure behave in similar manner, matching well with the experimental data. Since there is quantitative agreement with experimental data and both of the structures, the crystal structure was used for each of the structures investigated further in this study.

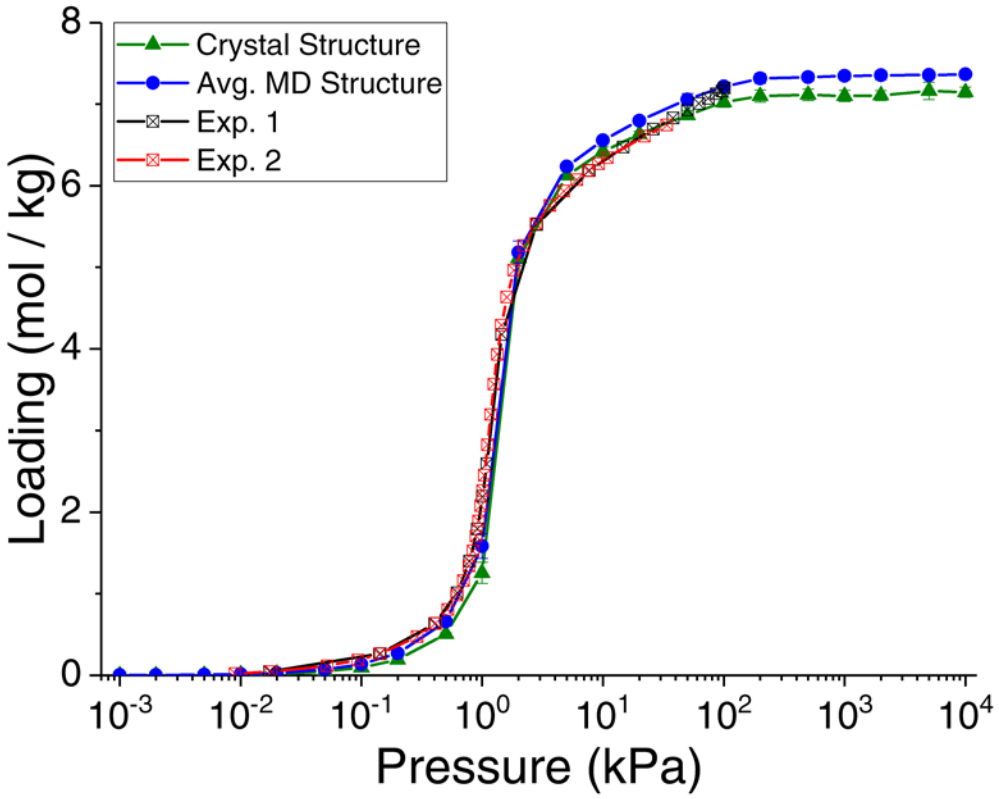

Figure S5: Comparison of experimental isotherms from this work of CO_2 in ITQ-29 at 195 K with the simulated adsorption isotherms using both the crystal structure of ITQ-29 and the average structure obtained from NPT MD simulations to account for temperature effects on the unit cell volume and framework window size.

Comparison of force field with experimental cation positions in 4A structure:

As a way to further check the CCFF force field, we performed parallel tempering of the cation positions, to compare the distributions of cations in the simulated results to the distribution given in the experimental crystal structure.[27] The final 10% of snapshots from GCMC simulations were analyzed to determine the distribution of cations relative to framework ring sizes. The results can be found in Table S4. The CCFF cation distributions and the crystal structure cation distributions are similar, showing the validity of using the CCFF force field in our study.

Table S4: Distributions of cations within the LTA-4A structure at different temperatures from 300 K to 600 K, with respect to the six-member ring windows (6MR), eight-member ring windows (8MR), four-member ring windows (4MR), and other positions in the framework. The experimental data is from Pluth and Smith[27] taken at room temperature.

LTA-4A Temp.	**6MR**	**8MR**	**4MR**	**Other**	**Total**
300 K	64	32	0	0	96
330 K	64	31.98 ± 0.14	0	0.02 ± 0.14	96 ± 0.28
360 K	64	32	0	0	96
390 K	64	31.96 ± 0.20	0	0.04 ± 0.20	96 ± 0.40
420 K	64	31.88 ± 0.33	0.06 ± 0.24	0.06 ± 0.24	96 ± 0.81
450 K	64	31.88 ± 0.33	0.04 ± 0.20	0.08 ± 0.27	96 ± 0.80
480 K	64	31.80 ± 0.40	0.10 ± 0.30	0.10 ± 0.30	96 ± 1.00
510 K	64	31.90 ± 0.30	0.02 ± 0.14	0.08 ± 0.27	96 ± 0.71
540 K	64	31.80 ± 0.45	0.02 ± 0.14	0.18 ± 0.18	96 ± 0.77
570 K	64	31.80 ± 0.45	0	0.20 ± 0.45	96 ± 0.90
600 K	64	31.53 ± 0.61	0.10 ± 0.30	0.37 ± 0.56	96 ± 1.47
Experiment	62	23	6	0	91.7 ± 1.0

Extending the temperature range of study for siliceous zeolites:

The small increase of the isosteric heat at zero loading near 300 K for ITQ-29 led us to examine the system at lower temperatures. ITQ-29 results for temperatures down to 10 K showed an increase of almost 12 kJ/mol, from ~18 kJ/mol at 600 K to ~30 kJ/mol at 10K. The same temperature range was examined with Si-CHA and Si-MFI to see if this change in heats of adsorption was specific to ITQ-29 or more general for siliceous zeolites or siliceous zeolites with 8MR windows. The Si-CHA does also show a large increase of around 8 kJ/mol over the 10 K – 600 K range. Si-MFI has a slight temperature dependence, with a change of around 6 kJ/mol over the same temperature range, compared to the difference in thermal energy of around 5 kJ/mol. The results for the three siliceous zeolites from 10 – 600 K range are presented in Figure 4. Further study of the ITQ-29 and Si-CHA systems concluded that the 30 kJ/mol heat of adsorption is due to CO_2 molecules located in the center of the 8MR window of these zeolites. The difference in thermal energy between 10 and 600 K is -4.9 kJ/mol, because the temperature contribution is subtracted from the values of the heats of adsorption (both at zero and non-zero loading) calculated by the RASPA program. If the values of the heat of adsorption were calculated to be the same at 10 and 600 K, the reported value would be smaller by 4.9 kJ/mol at 600 K compared to the value reported at 10 K.

Comparison between isosteric heats of adsorption calculated from fluctuation formula and Clausius-Clapeyron equation:

In order to make sure that the isosteric heats of adsorption obtained from the fluctuation method at different temperatures presented in Figure 1 of the main paper are reliable, the isosteric heats of adsorption were calculated using the Clausius-Clapeyron equation. Heats of adsorption were calculated using the formula:

$$-q = \left(\langle U \times N\rangle_\mu - \langle U\rangle_\mu \langle N\rangle_\mu\right)/\left(\langle N^2\rangle_\mu - \langle N\rangle_\mu \langle N\rangle_\mu\right) - \langle U_g\rangle - 1/\beta$$

where q is the heat of adsorption, $\langle \cdots \rangle_\mu$ denotes an average in the grand-canonical ensemble, U denotes the energy of a host, N is the number of guest molecules, μ is the chemical potential of the guest molecules, $\langle U_g\rangle$ is the average energy of an isolated guest molecule, and $\beta = 1/(k_B T)$.[28] For the LTA-4A systems, the temperatures of 300 K, 450 K, and 600 K were examined. In order to have isotherms that were not significantly influenced by numerical noise from the simulations, the temperature range used for Clausius-Clapeyron analysis with higher temperatures (450 K and 600 K) needed to be increased. For 300 K, a range of ± 5 K was enough to see different isotherms for the three temperatures. For 450 K, the range was extended to ± 10 K, and for 600 K, the range was extended to ± 30 K. The isosteric heats of adsorption from Clausius-Clapeyron analysis are shown below for 450 K and 600 K in Figures S6 and S7, respectively. An example of a siliceous system and the comparison between isosteric heats of adsorption from the fluctuation method and Clausius-Clapeyron analysis can be found below in Figure S8 for CO_2 in ITQ-29 at 195 K. In order to test the generality of the agreement of isosteric heats calculated by different methods, the isosteric heats of adsorption were calculated for CH_4 in ITQ-29 and the results are shown in Figure S9.

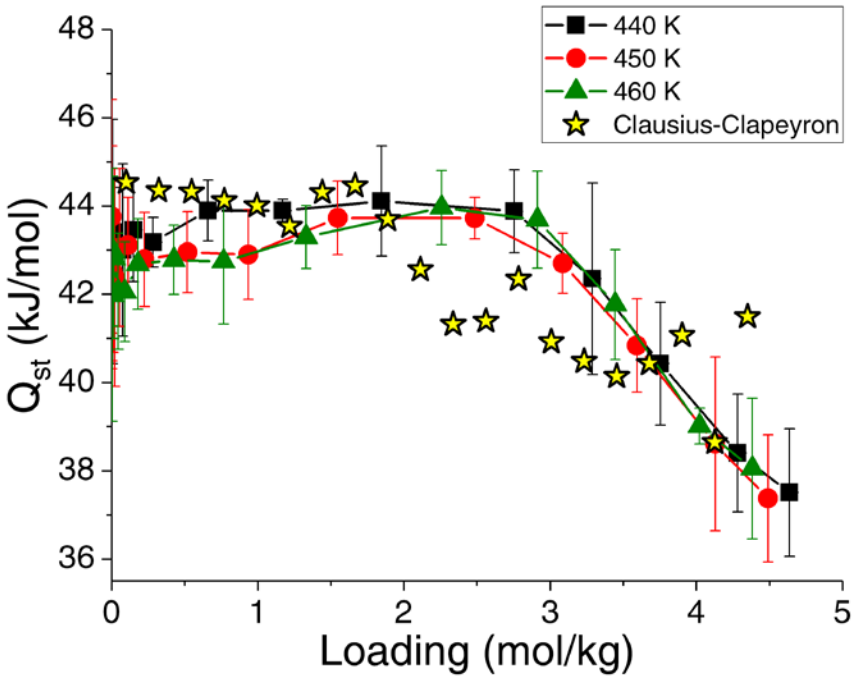

Figure S6: Isosteric heats of adsorption for CO_2 interacting with LTA-4A calculated by the fluctuation formula for 440 K, 450 K, and 460 K vs loading, along with the isosteric heat of adsorption obtained using the Clausius-Clapeyron equation (yellow and black stars) for the three temperatures presented in the graph.

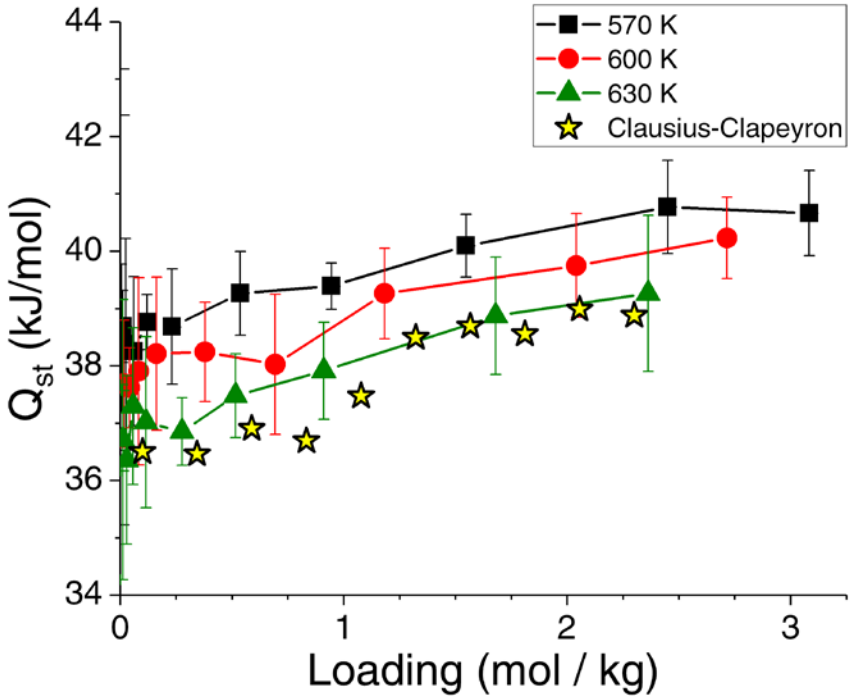

Figure S7: Isosteric heats of adsorption for CO_2 interacting with LTA-4A calculated by the fluctuation formula for 570 K, 600 K, and 630 K vs loading, along with the isosteric heat of adsorption obtained using the Clausius-Clapeyron equation (yellow and black stars) for the three temperatures presented in the graph.

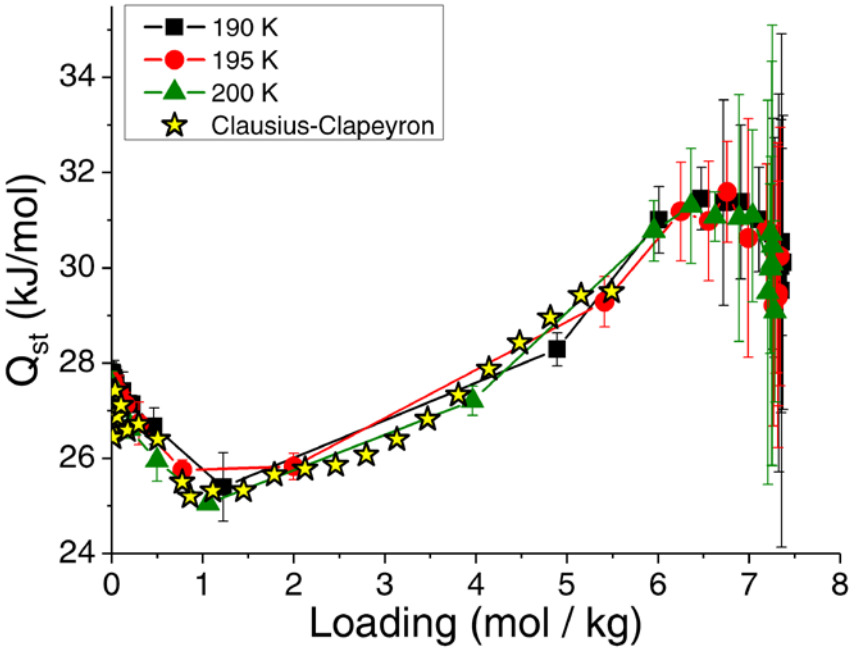

Figure S8: Isosteric heats of adsorption for CO_2 interacting with ITQ-29 calculated by the fluctuation formula for 190 K, 195 K, and 200 K vs loading, along with the isosteric heat of adsorption obtained using the Clausius-Clapeyron equation (yellow and black stars) for the three temperatures presented in the graph.

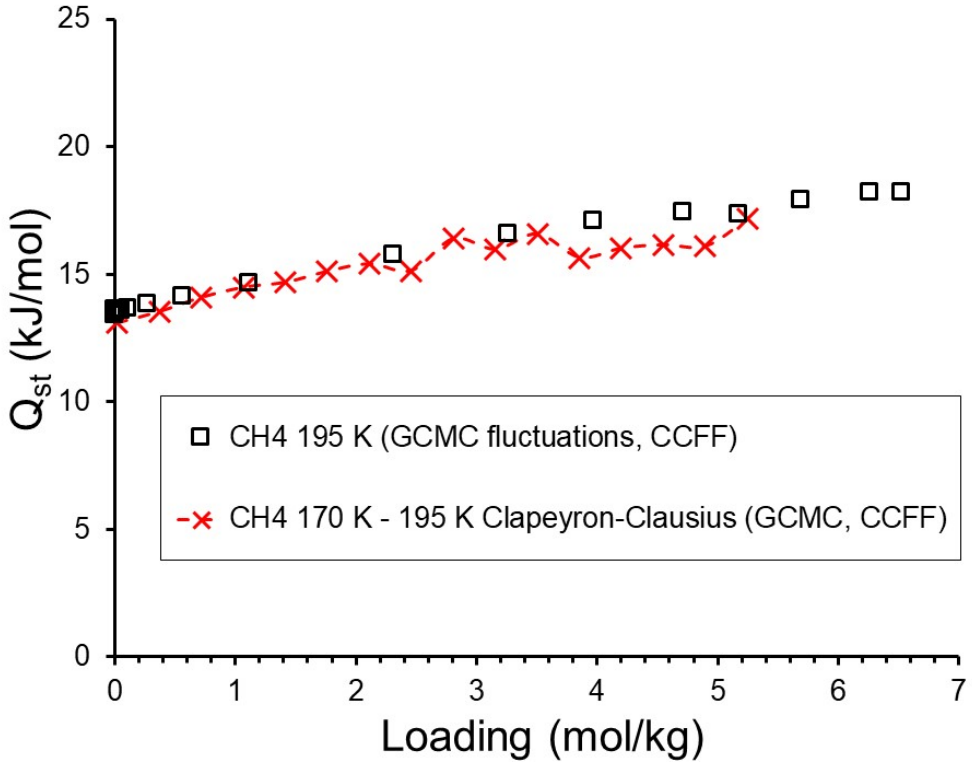

Figure S9. Comparison of the isosteric heats of adsorption of CH_4 in ITQ-29 calculated from GCMC simulations with the CCFF force field using the fluctuations formula (squares), and Clausius-Clapeyron equation using isotherms at 170 K and 195 K (line, crosses).

Comparison of the CO_2 positioning relative to cations:

For the cationic zeolites, the extra-framework cations will have the strongest interactions with the adsorbate molecules. The location of the CO_2 molecules with respect to the cation positions in the framework can help us understand the change in the heats of adsorption. We have calculated the distance of each CO_2 molecule present from snapshots in the Monte Carlo simulations and have set a distance parameter to decide whether a CO_2 molecule is close to a sodium atom, in the cationic zeolites, or the center of an n-membered ring, in the siliceous zeolites. In both cases, the distance selected was 3.5 Å, as this is close to the sum of the van der Waals radii of oxygen or carbon (form CO_2) and oxygen (from the zeolite) (3.14 Å for O-O and 3.22 Å for C-O), with a little extra distance included for potential interactions. With this in mind, the distance between the oxygen atoms of CO_2 and the sodium atoms or the carbon atom of CO_2 and the center of the n-membered rings was calculated. CO_2 molecules can be sitting in dual cation sites (both oxygen atoms are within 3.5 Å of Na cations), single cation sites (only one oxygen atom is within 3.5 Å of a Na cation), or a site with no cations (both oxygen atoms are greater than 3.5 Å away from a Na cation). The percentage of the CO_2 molecules sitting in each type of cation site in LTA-4A and Na-LTA with Si/Al = 2 are shown in Figure S10 and S12, respectively. The strengths of the interactions of CO_2 in the different cation sites of LTA-4A were investigated by using molecular dynamics (MD) simulations. MD simulations were

performed using the LAMMPS program[29] using the same CCFF force field as in the GCMC simulations for 2×10^7 steps, with a timestep of 1 fs. The loading of CO_2 molecules was held fixed at 1 molecule per α cage and the locations of the CO_2 molecules and energies were tracked at each MD step. The interaction energy per CO_2 molecule in different cation sites at 300 K is shown below in Figure S11. For the LTA-4A simulations, CO_2 adsorption distributions at 600 K show a reduction in the percentage of CO_2 molecules found in strongly interacting dual cation sites and an increase in the percentage of single cation and no cation occupations, compared to the adsorption distributions at 300 K. The distributions for Na-LTA with Si/Al = 2 show a similar trend to the distributions from LTA-4A, a reduction in the percentage of CO_2 molecules found in strongly interacting dual cation sites and an increase in the number of single cation and no cation occupations at 600 K, compared to adsorption at 303 K.

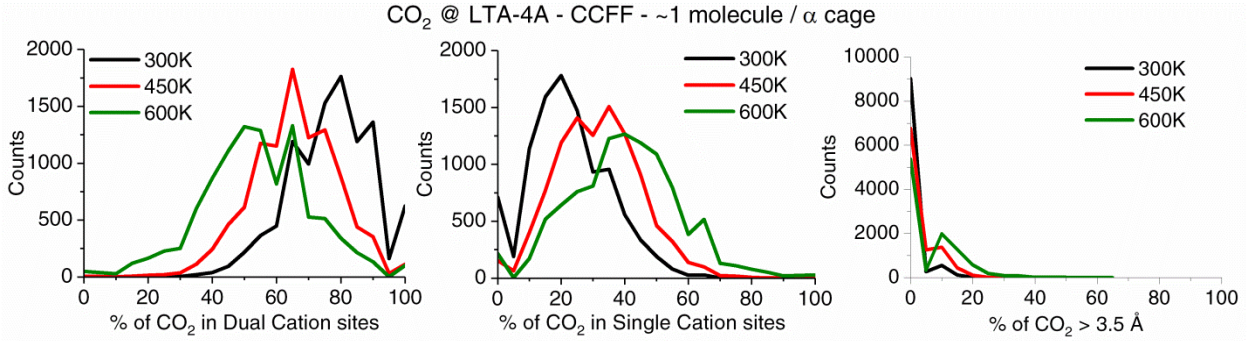

Figure S10: Comparison of the locations of CO_2 molecules relative to the cation positions in the LTA-4A structure. For each temperature, the pressure at which an average loading of at least one molecule per α-cage was selected. For 300, 450, and 600 K, the pressures selected are 2×10^2, 1×10^5 and 1×10^6 Pa, respectively.

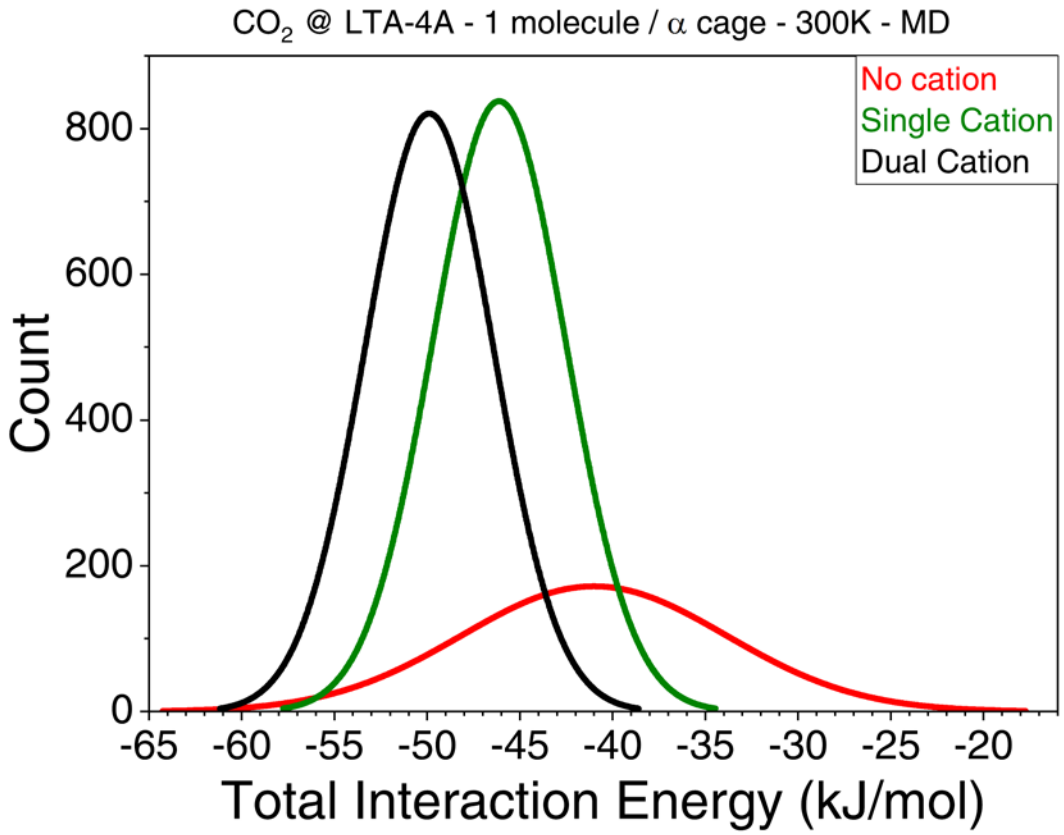

Figure S11: Comparison of the interaction energies of CO_2 in different cation sites in the LTA-4A structure from molecular dynamics simulations at 300 K. The interaction energies were separated into 1 kJ/mol bins before plotting. The average values for the interaction energies of CO_2 in dual, single and no cation sites in LTA-4A at 300 K are -50, -46, and -41 kJ/mol, respectively.

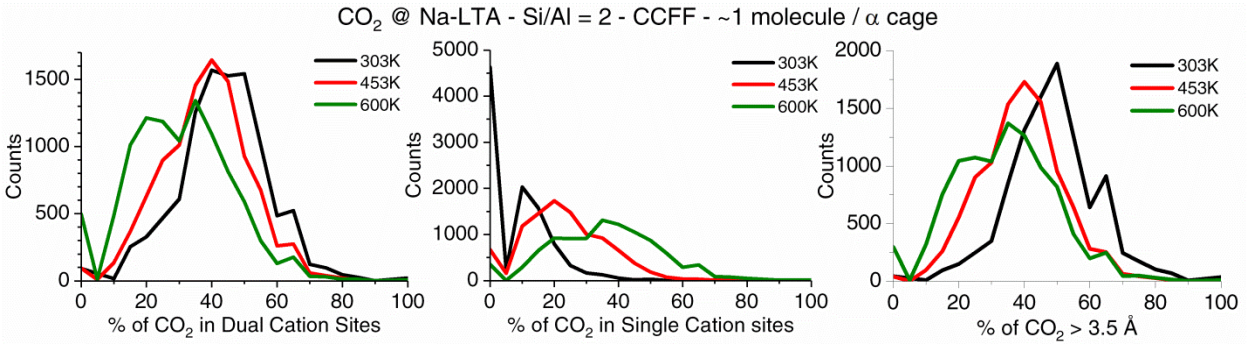

Figure S12: Comparison of the locations of CO_2 molecules relative to the cation positions in the Na-LTA with Si/Al = 2 structure. For each temperature, the pressure at which an average loading of at least one molecule per α-cage was selected. For 303, 453, and 600 K, the pressures selected are 2×10^3, 2×10^5 and 2×10^6 Pa, respectively.

Comparison of the CO_2 positioning relative to framework ring windows:

For the siliceous zeolites, which are free of cations, there is another way to describe the positioning of CO_2 molecules within the zeolite, namely the proximity to different ring window sizes in the framework. For the ITQ-29 and the siliceous-CHA frameworks, there are only 6, 8, and 4-member ring windows. The last 5% of snapshots from GCMC simulations were analyzed and the distributions of CO_2 molecules near different ring sizes are compared at each of the temperatures examined. The distributions of CO_2 molecules in ITQ-29 and siliceous-CHA can be found below in Figures S13 and S14, respectively.

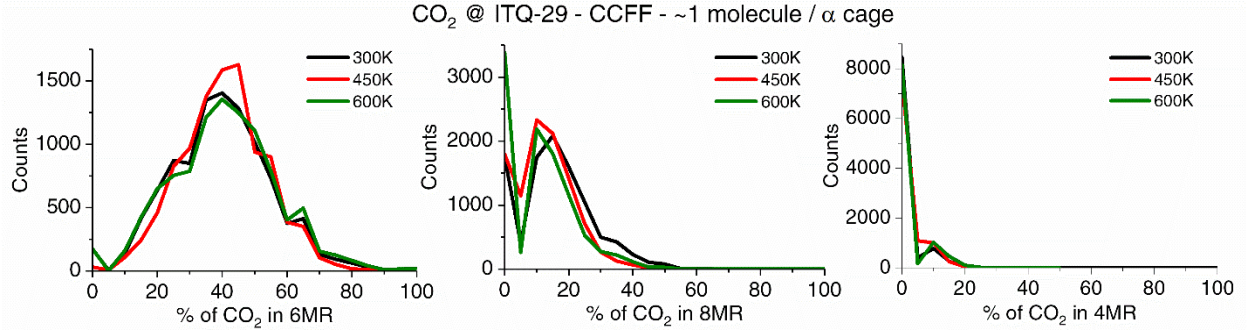

Figure S13: Comparison of the locations of CO_2 molecules relative to the 6MR, 8MR and 4MR windows in the ITQ-29 structure. For each temperature, the pressure at which an average loading of at least one molecule per α-cage was selected. For 300, 450, and 600 K, the pressures selected are 1×10^5, 2×10^6 and 5×10^6 Pa, respectively.

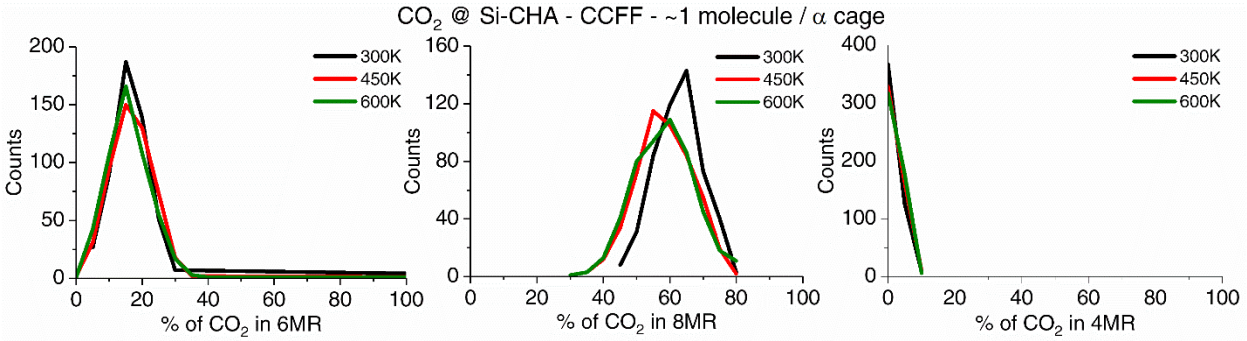

Figure S14: Comparison of the locations of CO_2 molecules relative to the 6MR, 8MR and 4MR windows in the siliceous-CHA structure for the last 5% of the GCMC simulations. For each temperature, the pressure at which an average loading of at least one molecule per unit cell was selected. For 300, 450, and 600 K, the pressures selected are 1×10^5, 2×10^6 and 1×10^7 Pa, respectively.

Table S5: Tabulated data for Figure 1 in the paper: Isotherms and heats of adsorption for CO_2 in LTA-4A.

	300 K		450 K		600 K	
Pressure (kPa)	Q_{st} (kJ/mol)	Loading (mol/kg)	Q_{st} (kJ/mol)	Loading (mol/kg)	Q_{st} (kJ/mol)	Loading (mol/kg)
0.001	47.3 ± 2.04	0.005	44.9 ± 34.9	1.540E-05	----	0.000E+00
0.002	47.3 ± 2.02	0.009	44.0 ± 32.7	2.713E-05	----	7.333E-07
0.005	47.8 ± 1.96	0.022	41.7 ± 18.9	5.206E-05	----	4.400E-06
0.01	48.1 ± 1.78	0.045	37.8 ± 12.6	1.071E-04	32.5 ± 41.1	1.100E-05
0.02	47.6 ± 1.17	0.089	43.7 ± 4.87	2.295E-04	40.4 ± 53.5	2.053E-05
0.05	47.9 ± 0.45	0.215	43.7 ± 7.14	6.196E-04	40.3 ± 43.4	3.886E-05
0.1	47.9 ± 0.46	0.433	43.8 ± 2.64	0.001	16.4 ± 18.2	8.506E-05
0.2	48.3 ± 1.26	0.835	42.8 ± 2.52	0.002	34.1 ± 10.3	1.716E-04
0.5	48.7 ± 1.13	1.683	42.5 ± 2.04	0.006	41.2 ± 7.58	4.583E-04
1	48.9 ± 1.04	2.345	42.3 ± 1.57	0.011	40.4 ± 9.64	8.631E-04
2	47.9 ± 0.97	2.962	42.4 ± 2.47	0.023	37.5 ± 7.26	0.002
5	45.7 ± 0.91	3.400	43.1 ± 1.79	0.057	35.7 ± 5.24	0.004
10	41.5 ± 0.83	3.643	43.1 ± 1.08	0.113	37.6 ± 3.33	0.008
20	38.3 ± 1.50	3.933	42.8 ± 1.07	0.225	37.7 ± 1.11	0.017
50	37.4 ± 1.61	4.485	42.9 ± 0.92	0.520	37.6 ± 0.70	0.042
100	36.2 ± 2.42	4.769	42.9 ± 1.02	0.936	37.9 ± 1.63	0.083
200	36.8 ± 1.47	5.155	43.7 ± 0.83	1.547	38.2 ± 1.34	0.162
500	34.7 ± 3.23	5.658	43.7 ± 0.47	2.485	38.2 ± 0.87	0.380
1,000	35.5 ± 1.18	5.966	42.7 ± 0.68	3.086	38.0 ± 1.22	0.694
2,000	35.3 ± 1.65	6.308	40.8 ± 1.06	3.594	39.3 ± 0.79	1.183
5,000	34.2 ± 1.81	6.561	38.6 ± 1.97	4.129	39.7 ± 0.90	2.041
10,000	33.0 ± 3.19	6.709	37.4 ± 1.44	4.490	40.2 ± 0.71	2.715

303K - Experiment				453 K - Experiment			
Isotherm		Heats of adsorption		Isotherm		Heats of adsorption	
Pressure (kPa)	Loading (mol/kg)	Loading (mol/kg)	Q_{st} (kJ/mol)	Pressure (kPa)	Loading (mol/kg)	Loading (mol/kg)	Q_{st} (kJ/mol)
0.066	0.598	0.600	47.750	0.0003	0.002	0.224	42.628
0.125	0.852	0.700	47.564	0.0018	0.004	0.262	41.079
0.263	1.313	0.800	47.453	0.0025	0.006	0.298	40.970
0.526	1.821	0.900	47.292	0.0028	0.008	0.332	41.061
0.800	2.116	1.000	47.193	0.0028	0.011	0.366	41.079
1.062	2.303	1.100	47.192	0.0028	0.013	0.398	41.117
1.344	2.442	1.200	47.569	0.0027	0.015	0.429	40.790
1.605	2.549	1.300	47.975	0.0027	0.018	0.460	40.502
1.897	2.639	1.400	47.743	0.0026	0.020	0.490	40.202
2.167	2.712	1.500	47.450	0.0026	0.022	0.519	40.412
2.420	2.764	1.600	47.354	0.0027	0.025	0.548	41.439

2.684	2.815	1.700	47.445	0.0028	0.027	0.574	40.940
5.342	3.116	1.800	47.569	0.0030	0.029	0.602	41.753
8.069	3.275	1.900	47.257	0.0033	0.031	0.627	40.852
10.853	3.397	2.000	46.909	0.0036	0.034	0.653	41.689
16.131	3.552	2.100	46.779	0.0041	0.036	0.678	40.675
21.555	3.666	2.200	46.534	0.0046	0.038	0.703	41.818
26.886	3.760	2.300	46.276	0.0053	0.040	0.726	39.848
32.276	3.838	2.400	45.720	0.0061	0.043	0.753	42.325
37.233	3.903	2.500	45.222	0.0071	0.045	0.773	41.137
42.654	3.960	2.600	44.931	0.0083	0.047	0.796	43.401
47.952	4.016			0.0097	0.049	0.818	40.836
53.406	4.057			0.0113	0.051	0.840	41.699
58.663	4.102			0.0569	0.066	0.860	40.301
64.065	4.146			0.1279	0.079	0.883	41.307
69.420	4.178			0.2096	0.090		
74.737	4.212			0.3013	0.099		
80.151	4.245			0.4014	0.106		
85.461	4.272			0.5085	0.113		
90.818	4.302			0.6217	0.119		
96.145	4.325			0.7407	0.125		
101.516	4.348			0.8651	0.130		
106.798	4.375			0.9917	0.135		
				1.1049	0.141		
				3.0496	0.184		
				5.0121	0.224		
				6.9831	0.262		
				8.9630	0.298		
				10.9506	0.332		
				12.9425	0.366		
				14.9351	0.398		
				16.9366	0.429		
				18.9361	0.460		
				20.9396	0.490		
				22.9424	0.519		
				24.9520	0.548		
				26.9728	0.574		
				28.9790	0.602		
				31.0067	0.627		
				33.0249	0.653		
				35.0507	0.678		
				37.0792	0.703		
				39.1158	0.726		
				41.1228	0.753		

		43.1750	0.773	
		45.2068	0.796	
		47.2514	0.818	
		49.2876	0.840	
		51.3358	0.860	
		53.3824	0.883	
		55.4403	0.902	
		57.4634	0.928	
		59.5167	0.948	
		61.5684	0.968	
		63.6980	0.975	
		65.8272	0.985	
		67.9133	1.006	
		69.9766	1.029	
		72.0583	1.049	
		74.1351	1.071	
		76.2037	1.093	
		78.2865	1.114	
		80.3462	1.136	
		82.4182	1.154	
		84.5143	1.168	
		86.6044	1.184	
		88.6848	1.204	
		90.7764	1.220	
		92.8639	1.238	
		94.9404	1.255	
		97.0263	1.271	
		99.1092	1.289	
		101.1918	1.307	

Table S6: Tabulated data for Figure 2 in the paper: Histograms of the interaction energy of CO_2 in LTA-4A.

300 K		**450 K**		**600 K**	
Interaction Energy / CO_2 molecule (kJ/mol)	Counts	Interaction Energy / CO_2 molecule (kJ/mol)	Counts	Interaction Energy / CO_2 molecule (kJ/mol)	Counts
-55	1	-52	2	-42	372
-54	7	-51	1	-41	596
-53	29	-50	9	-40	786
-52	118	-49	39	-39	936
-51	453	-48	95	-38	1103
-50	965	-47	212	-37	1041
-49	1728	-46	458	-36	1028
-48	2140	-45	875	-35	971
-47	1899	-44	1138	-34	783
-46	1321	-43	1417	-33	609
-45	746	-42	1585	-32	430
-44	345	-41	1366	-31	293
-43	150	-40	1081	-30	188
-42	63	-39	786	-29	126
-41	25	-38	456	-28	75
-40	5	-37	246	-27	43
-39	1	-36	119	-26	21
-38	2	-35	60	-25	16
-34	1	-34	33	-24	3
		-33	8	-23	2
		-32	9	-22	2
		-31	2	-21	2
		-30	1	-16	1
		-29	1	-14	1
				-8	1

Table S7: Tabulated data for Figure 3 in the paper: Heats of adsorption and loadings of CO_2 in LTA-4A from GCMC simulations and Clausius-Clapeyron analysis.

	295 K		300 K		305 K	
Pressure (kPa)	Q_{st} (kJ/mol)	Loading (mol/kg)	Q_{st} (kJ/mol)	Loading (mol/kg)	Q_{st} (kJ/mol)	Loading (mol/kg)
0.001	48.5 ± 2.53	0.007 ± 0.001	47.3 ± 2.04	0.005 ± 0.001	47.5 ± 2.34	0.004 ± 4.2E-04
0.002	49.3 ± 2.45	0.014 ± 0.002	47.3 ± 2.02	0.009 ± 0.001	47.6 ± 3.79	0.008 ± 3.9E-04
0.005	48.1 ± 1.99	0.037 ± 0.002	47.8 ± 1.96	0.022 ± 0.001	47.8 ± 1.64	0.020 ± 0.001
0.01	49.2 ± 1.27	0.073 ± 0.004	48.1 ± 1.78	0.045 ± 0.004	48.8 ± 0.71	0.039 ± 0.003
0.02	48.8 ± 1.08	0.146 ± 0.010	47.6 ± 1.17	0.089 ± 0.005	47.6 ± 0.70	0.080 ± 0.005
0.05	49.3 ± 0.65	0.353 ± 0.032	47.9 ± 0.45	0.215 ± 0.010	48.2 ± 0.72	0.191 ± 0.006
0.1	49.4 ± 0.37	0.693 ± 0.038	47.9 ± 0.46	0.433 ± 0.022	48.5 ± 1.32	0.365 ± 0.019
0.2	49.4 ± 0.50	1.207 ± 0.039	48.3 ± 1.26	0.835 ± 0.043	48.7 ± 0.52	0.714 ± 0.012
0.5	49.6 ± 1.84	2.163 ± 0.097	48.7 ± 1.13	1.683 ± 0.043	48.9 ± 1.20	1.472 ± 0.068
1	49.8 ± 0.56	2.795 ± 0.062	48.9 ± 1.04	2.345 ± 0.064	49.2 ± 1.06	2.160 ± 0.055
2	47.9 ± 1.56	3.185 ± 0.056	47.9 ± 0.97	2.962 ± 0.063	48.7 ± 1.33	2.781 ± 0.020
5	43.2 ± 3.03	3.557 ± 0.035	45.7 ± 0.91	3.400 ± 0.063	46.6 ± 1.97	3.317 ± 0.025
10	42.2 ± 2.23	3.854 ± 0.089	41.5 ± 0.83	3.643 ± 0.062	43.2 ± 2.24	3.601 ± 0.043
20	38.0 ± 1.13	4.061 ± 0.087	38.3 ± 1.50	3.933 ± 0.115	39.7 ± 1.35	3.852 ± 0.029
50	35.9 ± 2.00	4.464 ± 0.064	37.4 ± 1.61	4.485 ± 0.053	37.5 ± 2.32	4.237 ± 0.078
100	35.7 ± 1.44	4.904 ± 0.021	36.2 ± 2.42	4.769 ± 0.130	35.2 ± 1.44	4.528 ± 0.021
200	35.1 ± 2.18	5.220 ± 0.095	36.8 ± 1.47	5.155 ± 0.091	34.9 ± 1.86	4.859 ± 0.034
500	34.8 ± 1.02	5.647 ± 0.132	34.7 ± 3.23	5.658 ± 0.065	34.5 ± 1.80	5.255 ± 0.074
1,000	35.6 ± 2.53	6.069 ± 0.143	35.5 ± 1.18	5.966 ± 0.095	34.7 ± 1.94	5.587 ± 0.064
2,000	35.0 ± 1.02	6.297 ± 0.057	35.3 ± 1.65	6.308 ± 0.066	34.1 ± 2.44	5.950 ± 0.094
5,000	35.5 ± 0.83	6.641 ± 0.113	34.2 ± 1.81	6.561 ± 0.079	34.6 ± 4.77	6.259 ± 0.158
10,000	33.8 ± 3.82	6.755 ± 0.088	33.0 ± 3.19	6.709 ± 0.123	34.6 ± 1.43	6.456 ± 0.081

Clausius-Clapeyron	
Loading (mol/kg)	Q_{st} (kJ/mol)
0.100	49.373
0.589	49.335
1.078	50.241
1.567	49.180
2.056	49.947
2.544	50.218
3.033	52.497
3.522	49.176
4.011	40.545
4.500	41.372

Table S8: Tabulated data for Figure 4 in the paper: Heats of adsorption at infinite dilution for CO_2 in different cationic and siliceous zeolites.

	LTA-4A	**Na-LTA Si/Al = 2**	**Na-LTA Si/Al = 5**	**Si-MFI**	**Si-CHA**	**ITQ-29**
Temp. (K)	Q_{st}^0 (kJ/mol)	Q_{st}^0 (kJ/mol)	Q_{st}^0 (kJ/mol)	Q_{st}^0 (kJ/mol)	Q_{st}^0 (kJ/mol)	Q_{st}^0 (kJ/mol)
300	47.9 ± 1.97	----	45.1 ± 3.66	26.5 ± 0.01	23.7 ± 0.00	20.6 ± 0.07
303	----	46.8 ± 1.20	----	----	23.7 ± 0.01	----
330	45.5 ± 1.76	----	44.6 ± 3.48	26.2 ± 0.01	----	19.5 ± 0.01
333	----	45.8 ± 0.39	----	----	23.3 ± 0.01	----
360	44.7 ± 2.82	----	42.7 ± 1.40	25.9 ± 0.01	----	18.7 ± 0.03
363	----	----	----	----	23.1 ± 0.01	----
390	44.5 ± 1.31	----	40.8 ± 2.83	25.7 ± 0.01	----	18.2 ± 0.01
393	----	43.8 ± 0.28	----	----	22.9 ± 0.01	----
420	43.5 ± 1.08	----	37.6 ± 1.80	25.5 ± 0.01	22.8 ± 0.01	17.9 ± 0.02
450	41.9 ± 1.12	----	35.9 ± 0.87	25.4 ± 0.01	22.7 ± 0.01	17.7 ± 0.01
453	----	41.2 ± 0.88	----	----	----	----
480	40.9 ± 0.80	----	34.4 ± 1.89	25.2 ± 0.01	22.6 ± 0.01	17.6 ± 0.01
503	----	39.2 ± 0.29	----	----	----	----
510	39.8 ± 0.81	----	33.1 ± 0.61	25.2 ± 0.02	22.5 ± 0.01	17.6 ± 0.01
540	38.5 ± 0.26	----	31.7 ± 0.40	25.1 ± 0.01	22.5 ± 0.01	17.6 ± 0.01
570	37.7 ± 0.64	----	30.6 ± 0.50	25.1 ± 0.02	22.5 ± 0.01	17.7 ± 0.01
600	36.8 ± 0.65	35.6 ± 0.37	29.7 ± 0.35	25.1 ± 0.00	22.6 ± 0.01	17.7 ± 0.01
			Experiment			
195	----	----	----	----	----	27.2
300	----	----	----	----	----	20
333	47.5	----	----	----	----	----
393	45	----	----	----	----	15
453	42.5	----	----	----	----	----
503	40	----	----	----	----	----

Table S9: Tabulated data for Figure 5 in the paper: Heats of adsorption at infinite dilution for CH_4 in different cationic and siliceous zeolites.

	LTA-4A	**Na-LTA Si/Al = 2**	**Na-LTA Si/Al = 5**	**Si-MFI**	**Si-CHA**	**ITQ-29**
Temp. (K)	Q_{st}^0 (kJ/mol)	Q_{st}^0 (kJ/mol)	Q_{st}^0 (kJ/mol)	Q_{st}^0 (kJ/mol)	Q_{st}^0 (kJ/mol)	Q_{st}^0 (kJ/mol)
170	----	----	----	----	----	13.1 ± 0.01
195	----	----	----	----	----	13.2 ± 0.01
209	----	----	----	----	16.2 ± 0.001	----
243	----	----	----	----	16.3 ± 0.002	----
273	----	----	----	----	16.4 ± 0.002	----
300	18.0 ± 0.01	16.4 ± 0.03	15.1 ± 0.02	19.3 ± 0.004	16.6 ± 0.002	13.6 ± 0.002
303	----	----	----	----	16.6 ± 0.001	----
333	----	----	----	----	16.7 ± 0.002	----
363	----	----	----	----	16.9 ± 0.002	----
393	----	----	----	----	17.0 ± 0.002	----
450	17.8 ± 0.02	16.4 ± 0.01	15.2 ± 0.02	19.8 ± 0.004	17.3 ± 0.002	14.5 ± 0.003
600	18.3 ± 0.02	17.0 ± 0.02	15.9 ± 0.03	20.4 ± 0.01	18.2 ± 0.003	15.4 ± 0.01

Table S10: Tabulated data for Figure 6 in paper: Heats of adsorption at infinite dilution for N_2 in different cationic and siliceous zeolites.

	LTA-4A	**Na-LTA Si/Al = 2**	**Na-LTA Si/Al = 5**	**Si-MFI**	**Si-CHA**	**ITQ-29**
Temp. (K)	Q_{st}^0 (kJ/mol)	Q_{st}^0 (kJ/mol)	Q_{st}^0 (kJ/mol)	Q_{st}^0 (kJ/mol)	Q_{st}^0 (kJ/mol)	Q_{st}^0 (kJ/mol)
300	17.1 ± 0.07	15.8 ± 0.11	15.2 ± 0.04	16.8 ± 0.00	14.8 ± 0.003	12.1 ± 0.00
450	15.1 ± 0.05	14.4 ± 0.03	13.8 ± 0.03	17.2 ± 0.00	15.4 ± 0.003	12.8 ± 0.00
600	14.7 ± 0.05	14.3 ± 0.02	14.0 ± 0.03	17.8 ± 0.01	16.2 ± 0.003	13.7 ± 0.00

Table S11: Tabulated data for Figure 7 in paper: CO_2 positions in Na-LTA with Si/Al = 5.

300 K						**450 K**					
% of CO_2 molecules in dual cation sites	Counts	% of CO_2 molecules in single cation sites	Counts	% of CO_2 molecules with O-Na distances > 3.5 Å	Counts	% of CO_2 molecules in dual cation sites	Counts	% of CO_2 molecules in single cation sites	Counts	% of CO_2 molecules with O-Na distances > 3.5 Å	Counts
0	3	0	203	0	2246	0	640	0	157	0	1247
5	0	5	5	5	361	5	12	5	0	5	16
10	4	10	470	10	2775	10	539	10	63	10	772
15	11	15	589	15	1868	15	1219	15	280	15	1537
20	54	20	1093	20	1458	20	1329	20	367	20	1374
25	113	25	1230	25	749	25	1234	25	448	25	1111
30	203	30	1081	30	298	30	990	30	511	30	895
35	539	35	1537	35	174	35	1222	35	874	35	1029

40	863	40	1368	40	56	40	980	40	1082	40	809
45	1287	45	1064	45	12	45	663	45	1177	45	471
50	1337	50	588	50	2	50	587	50	1368	50	399
55	1519	55	397	55	1	55	210	55	1008	55	137
60	1130	60	187	60	0	60	117	60	588	60	72
65	1307	65	129	65	0	65	146	65	957	65	80
70	526	70	32	70	0	70	23	70	326	70	11
75	454	75	20	75	0	75	35	75	295	75	17
80	371	80	4	80	0	80	24	80	215	80	15
85	122	85	1	85	0	85	10	85	160	85	4
90	114	90	2	90	0	90	1	90	51	90	1
95	0	95	0	95	0	95	0	95	0	95	0
100	43	100	0	100	0	100	19	100	73	100	3

600 K

% of CO_2 molecules in dual cation sites	Counts	% of CO_2 molecules in single cation sites	Counts	% of CO_2 molecules with O-Na distances > 3.5 Å	Counts
0	1832	0	58	0	226
5	242	5	0	5	5
10	1978	10	70	10	266
15	1874	15	210	15	563
20	1610	20	325	20	790
25	994	25	478	25	1019
30	553	30	524	30	953
35	443	35	901	35	1356
40	222	40	1106	40	1353
45	115	45	1255	45	1128
50	100	50	1274	50	895
55	15	55	1118	55	625
60	9	60	686	60	289
65	9	65	948	65	303
70	1	70	381	70	88
75	2	75	282	75	72
80	0	80	180	80	34
85	0	85	96	85	16
90	0	90	69	90	8
95	0	95	0	95	0
100	1	100	39	100	11

Table S12: Tabulated data for Figure 8 in paper: CO_2 positions in Si-MFI.

300 K				450 K				600 K			
% of CO_2 molecules in 6MR sites	Counts	% of CO_2 molecules in 10MR sites	Counts	% of CO_2 molecules in 6MR sites	Counts	% of CO_2 molecules in 10MR sites	Counts	% of CO_2 molecules in 6MR sites	Counts	% of CO_2 molecules in 10MR sites	Counts
0	9566	0	701	0	9266	0	387	0	9233	0	493
5	56	5	29	5	243	5	65	5	141	5	60
10	242	10	546	10	381	10	704	10	455	10	734
15	112	15	1184	15	97	15	1053	15	153	15	1140
20	18	20	1309	20	10	20	1433	20	16	20	1352
25	1	25	1262	25	2	25	1536	25	2	25	1361
30	5	30	904	30	0	30	1176	30	0	30	1083
35	0	35	1205	35	0	35	1236	35	0	35	1251
40	0	40	947	40	1	40	950	40	0	40	944
45	0	45	734	45	0	45	674	45	0	45	662
50	0	50	557	50	0	50	403	50	0	50	475
55	0	55	237	55	0	55	205	55	0	55	207
60	0	60	147	60	0	60	65	60	0	60	97
65	0	65	146	65	0	65	80	65	0	65	95
70	0	70	35	70	0	70	11	70	0	70	14
75	0	75	23	75	0	75	8	75	0	75	15
80	0	80	11	80	0	80	10	80	0	80	8
85	0	85	10	85	0	85	2	85	0	85	5
90	0	90	1	90	0	90	0	90	0	90	0
95	0	95	0	95	0	95	0	95	0	95	0
100	0	100	12	100	0	100	2	100	0	100	4

Table S13: Tabulated data for Figure S1: Comparison of literature force fields with CCFF used in this study and experimental data obtained by calorimetric experiments during this study. The σ value in the table refers to the σ for the oxygen atoms in the zeolite in each force field.

	Loading (mol/kg)										
Pressure (kPa)	**σ = 3.101**	**σ = 3**	**σ = 3.04**	**σ = 3.6**	**σ = 2.789**	**σ = 3.001**	**σ = 2.806**	**σ = 3.011**	**σ = 3.5532**	**σ = 3.34**	**σ = 3.265**
0.001	0.002	3.47E-06	4.126	0.018	0.002	0.001	0.002	0.001	0.003	0.001	0.002
0.002	0.003	2.60E-06	4.989	0.037	0.004	0.002	0.003	0.002	0.006	0.001	0.005
0.005	0.008	6.07E-06	5.582	0.093	0.010	0.005	0.008	0.006	0.015	0.003	0.012
0.01	0.016	2.17E-05	5.895	0.192	0.019	0.011	0.015	0.012	0.030	0.006	0.024
0.02	0.031	5.46E-05	6.054	0.402	0.038	0.021	0.030	0.023	0.057	0.011	0.050
0.05	0.078	1.27E-04	6.157	1.049	0.097	0.055	0.073	0.060	0.139	0.029	0.126
0.1	0.153	2.61E-04	6.212	1.828	0.184	0.115	0.145	0.119	0.283	0.055	0.245
0.2	0.299	0.001	6.216	2.617	0.345	0.253	0.276	0.241	0.525	0.113	0.481
0.5	0.776	0.001	6.278	3.487	0.767	0.881	0.641	0.670	1.336	0.298	1.410
1	1.997	0.003	6.239	3.864	1.446	2.535	1.234	2.255	4.157	0.776	4.935
2	5.411	0.005	6.240	4.033	3.581	4.104	3.211	5.915	5.785	4.965	5.900
5	6.249	0.013	6.270	4.121	6.060	4.947	6.028	6.648	6.352	6.135	6.358
10	6.555	0.027	6.473	4.140	6.572	5.479	6.567	6.936	6.616	6.455	6.551
20	6.758	0.055	6.551	4.149	6.891	5.997	6.889	7.172	6.805	6.657	6.709
50	6.989	0.147	6.571	4.155	7.192	6.423	7.179	7.400	7.021	6.911	6.922
100	7.192	0.346	6.503	4.158	7.345	6.803	7.379	7.486	7.113	7.025	6.973
200	7.287	0.975	6.431	4.160	7.481	6.950	7.483	7.546	7.283	7.103	7.121
500	7.309	0.963	6.436	4.160	7.493	6.886	7.474	7.574	7.312	7.155	7.082
1,000	7.268	1.001	6.444	4.160	7.466	7.002	7.484	7.562	7.248	7.127	7.177
2,000	7.318	1.058	6.510	4.160	7.495	6.991	7.482	7.581	7.284	7.140	7.178
5,000	7.319	1.250	6.536	4.160	7.473	7.025	7.498	7.579	7.293	7.165	7.149
10,000	7.340	1.684	6.738	4.159	7.496	7.008	7.508	7.578	7.270	7.210	7.179

Experiment			
Pressure (kPa)	Loading (mol/kg)	Pressure (kPa)	Loading (mol/kg)
0.02	0.047	0.01	0.022
0.14	0.267	0.02	0.044
0.41	0.634	0.05	0.115
0.62	1.012	0.09	0.188
0.79	1.400	0.14	0.260
0.91	1.795	0.29	0.474
1.01	2.193	0.41	0.639
1.09	2.592	0.52	0.809
1.46	4.175	0.62	0.984
2.83	5.522	0.70	1.162
7.74	6.188	0.78	1.342
14.66	6.472	0.84	1.524
26.11	6.694	0.89	1.708

38.01	6.829	0.94	1.894
50.07	6.930	0.97	2.080
62.24	7.008	1.01	2.266
74.49	7.070	1.04	2.452
86.77	7.127	1.11	2.826
96.80	7.161	1.18	3.198
101.26	7.197	1.25	3.567
		1.34	3.931
		1.45	4.288
		1.60	4.634
		1.83	4.964
		2.21	5.268
		2.79	5.535
		3.64	5.756
		4.75	5.933
		6.08	6.072
		7.57	6.181
		9.17	6.270
		10.86	6.344
		22.00	6.606
		33.77	6.744

Table S14: Tabulated for Figure S2: Difference between literature force fields and CCFF used in this study. The σ value in the table refers to the σ for the oxygen atoms in the zeolite in each force field.

Pressure (kPa)	Difference between loading from literature force fields and CCFF (mol/kg)										
	σ = 3.101	**σ = 3**	**σ = 3.04**	**σ = 3.6**	**σ = 2.789**	**σ = 3.001**	**σ = 2.806**	**σ = 3.011**	**σ = 3.5532**	**σ = 3.34**	**σ = 3.265**
0.001	0.000	-0.002	4.124	0.017	4.80E-04	-4.50E-04	-4.00E-05	-4.00E-04	0.001	-9.85E-04	9.20E-04
0.002	0.000	-0.003	4.986	0.034	9.70E-04	-8.70E-04	7.00E-05	-7.60E-04	0.003	-0.002	0.002
0.005	0.000	-0.008	5.575	0.086	0.002	-0.002	2.80E-04	-0.002	0.007	-0.005	0.005
0.01	0.000	-0.016	5.879	0.176	0.003	-0.005	-9.80E-04	-0.004	0.014	-0.010	0.008
0.02	0.000	-0.030	6.023	0.371	0.008	-0.009	-3.20E-04	-0.007	0.026	-0.019	0.019
0.05	0.000	-0.078	6.079	0.972	0.019	-0.022	-0.005	-0.018	0.061	-0.049	0.048
0.1	0.000	-0.153	6.059	1.674	0.031	-0.038	-0.008	-0.035	0.129	-0.098	0.092
0.2	0.000	-0.299	5.917	2.318	0.046	-0.046	-0.023	-0.058	0.226	-0.187	0.182
0.5	0.000	-0.775	5.502	2.711	-0.010	0.105	-0.135	-0.106	0.560	-0.478	0.634
1	0.000	-1.995	4.242	1.867	-0.552	0.538	-0.763	0.257	2.160	-1.221	2.938
2	0.000	-5.406	0.829	-1.379	-1.830	-1.307	-2.200	0.504	0.374	-0.446	0.489
5	0.000	-6.236	0.020	-2.129	-0.189	-1.302	-0.222	0.398	0.102	-0.114	0.108
10	0.000	-6.528	-0.082	-2.415	0.017	-1.076	0.011	0.381	0.061	-0.100	-0.004
20	0.000	-6.704	-0.207	-2.610	0.132	-0.762	0.130	0.414	0.047	-0.101	-0.049
50	0.000	-6.842	-0.418	-2.834	0.203	-0.566	0.190	0.411	0.032	-0.078	-0.067
100	0.000	-6.846	-0.689	-3.034	0.153	-0.389	0.187	0.294	-0.079	-0.167	-0.219
200	0.000	-6.312	-0.857	-3.128	0.194	-0.337	0.196	0.259	-0.005	-0.184	-0.166
500	0.000	-6.346	-0.873	-3.149	0.184	-0.423	0.166	0.266	0.003	-0.153	-0.227
1,000	0.000	-6.267	-0.824	-3.108	0.198	-0.266	0.216	0.294	-0.021	-0.141	-0.091
2,000	0.000	-6.260	-0.807	-3.158	0.177	-0.327	0.164	0.263	-0.034	-0.178	-0.140
5,000	0.000	-6.070	-0.783	-3.159	0.154	-0.294	0.179	0.260	-0.026	-0.154	-0.171
10,000	0.000	-5.656	-0.602	-3.181	0.156	-0.332	0.167	0.237	-0.070	-0.130	-0.161

Table S15: Comparison of simulated (CCFF) and experimental adsorption isotherms and heats of adsorption of CH_4 in (a and b) LTA-4A, (c and d) Na-LTA with Si/Al = 2, and (e and f) Na-LTA with Si/Al = 5. The experimental data are from Harper et al.,[21] Li et al.,[22] Ahmed et al.,[23] Eagan et al.,[24] Jensen et al.,[25] and Palomino et al.[26]

CH_4 in LTA-4A

CCFF (303 K)		**Exp. Harper (303 K)**		**Exp. Li (301 K)**		**Exp. Ahmed (301 K)**	
Pressure (kPa)	Loading (mol/kg)	Pressure (kPa)	Loading (mol/kg)	Pressure (kPa)	Loading (mol/kg)	Pressure (kPa)	Loading (mol/kg)
0.001	1.10E-05	24.938	0.175	7.229	0.092	33.290	0.314
0.005	2.49E-05	50.055	0.347	15.663	0.164	59.119	0.483
0.01	7.63E-05	73.992	0.484	26.305	0.261	92.983	0.632
0.05	3.11E-04	98.775	0.657	38.956	0.381	123.404	0.726
0.1	0.001			57.831	0.483	154.972	0.801
0.5	0.003			88.353	0.656	188.263	0.845
1	0.007					211.221	0.861
5	0.033						
10	0.065						
20	0.129						
40	0.253						
60	0.371						
80	0.485						
100	0.594						
200	1.061						
300	1.418						
400	1.706						
500	1.929						
800	2.399						
1000	2.605						

CH_4 in LTA-4A

CCFF (303 K)		**Exp. Harper (303 K)**		**Exp. Eagan (253 - 273 K)**		**Exp. Jensen (248 - 302 K)**	
Loading (mol/kg)	Q_{st} (kJ/mol)	Loading (mol/kg)	Q_{st} (kJ/mol)	Loading (mol/kg)	Q_{st} (kJ/mol)	Loading (mol/kg)	Q_{st} (kJ/mol)
0.003	18.206 ± 2.413	0.223	16.736	0.201	20.200	0.066	17.570
0.033	18.417 ± 0.509	0.446	16.318	0.452	20.200	0.182	18.318
0.065	18.491 ± 0.205	1.339	14.853	0.648	19.850	0.284	18.505
0.129	18.655 ± 0.481	2.232	14.016	0.884	20.200	0.393	19.065
0.253	18.769 ± 0.187			1.094	19.499	0.503	19.252
0.371	18.783 ± 0.254			1.332	19.266		
0.485	19.042 ± 0.101			1.555	19.032		
0.594	19.111 ± 0.218			1.779	19.032		
1.061	19.661 ± 0.116			2.002	18.565		
1.418	20.076 ± 0.227			2.225	18.565		
1.706	20.303 ± 0.407						
1.929	20.619 ± 0.221						
2.399	21.066 ± 0.203						
2.605	21.248 ± 0.201						

CH_4 in Na-LTA (Si/Al = 2)							
CCFF (303 K)		**Exp. Palomino (303 K)**		**CCFF (303 K)**		**Exp. Palomino (273 - 303 K)**	
Pressure (kPa)	Loading (mol/kg)	Pressure (kPa)	Loading (mol/kg)	Loading (mol/kg)	Q_{st} (kJ/mol)	Loading (mol/kg)	Q_{st} (kJ/mol)
0.001	4.64E-06	2.626	0.033	0.002	17.238 ± 1.848	0.002	15.252
0.005	2.71E-05	5.033	0.044	0.023	17.228 ± 0.486	0.017	15.957
0.01	4.79E-05	7.221	0.054	0.046	17.327 ± 0.503	0.031	16.459
0.05	2.12E-04	9.190	0.064	0.091	17.248 ± 0.359	0.046	16.861
0.1	4.50E-04	10.722	0.071	0.180	17.286 ± 0.136	0.064	16.959
0.5	0.002	12.254	0.078	0.265	17.203 ± 0.245	0.086	17.157
1	0.005	14.442	0.089	0.349	17.459 ± 0.130	0.104	17.457
5	0.023	16.193	0.097	0.428	17.365 ± 0.086	0.127	17.756
10	0.046	17.505	0.103	0.793	17.776 ± 0.362	0.149	17.955
20	0.091	18.818	0.110	1.099	18.072 ± 0.183	0.171	18.153
40	0.180	20.350	0.117	1.357	18.314 ± 0.238	0.192	18.251
60	0.265	22.538	0.127	1.574	18.475 ± 0.157	0.209	18.349
80	0.349	25.383	0.141			0.225	18.548
100	0.428	28.009	0.153			0.245	18.747
200	0.793	30.635	0.166			0.263	18.845
300	1.099	33.479	0.179			0.285	19.043
400	1.357	36.105	0.192			0.303	19.242
500	1.574	38.512	0.203			0.323	19.340
		41.138	0.216			0.339	19.539
		44.639	0.232			0.359	19.839
		46.827	0.243			0.376	19.937
		53.173	0.273			0.394	20.035
		60.394	0.307			0.412	20.335
		66.740	0.337			0.431	20.433
		98.468	0.488			0.449	20.530
		100.438	0.497			0.466	20.629
						0.481	20.626

CH_4 in Na-LTA (Si/Al = 5)							
CCFF (303 K)		**Exp. Palomino (303 K)**		**CCFF (303 K)**		**Exp. Palomino (273 - 303 K)**	
Pressure (kPa)	Loading (mol/kg)	Pressure (kPa)	Loading (mol/kg)	Loading (mol/kg)	Q_{st} (kJ/mol)	Loading (mol/kg)	Q_{st} (kJ/mol)
0.001	4.90E-06	2.626	0.009	3.31E-04	15.178 ± 2.664	0.010	16.867
0.005	1.63E-05	5.033	0.017	0.002	15.952 ± 2.161	0.029	16.965
0.01	2.29E-05	7.221	0.024	0.003	15.721 ± 1.007	0.052	16.961
0.05	1.63E-04	9.190	0.031	0.016	15.776 ± 0.076	0.072	16.857
0.1	3.31E-04	10.722	0.036	0.032	15.701 ± 0.255	0.092	16.954
0.5	0.002	12.254	0.041	0.064	15.591 ± 0.284	0.110	16.951
1	0.003	14.442	0.048	0.127	15.600 ± 0.192	0.133	16.745
5	0.016	16.193	0.054	0.189	15.800 ± 0.108	0.152	16.641
10	0.032	17.505	0.059	0.249	15.838 ± 0.111	0.172	16.638
20	0.064	18.818	0.063	0.306	15.869 ± 0.216	0.195	16.634
40	0.127	19.915	0.067	0.582	16.053 ± 0.215	0.212	16.631
60	0.189	21.228	0.071	0.832	16.292 ± 0.123	0.231	16.729
80	0.249	22.760	0.076	1.053	16.500 ± 0.126	0.253	16.624

100	0.306	25.386	0.085	1.251	16.629 ± 0.151	0.269	16.722
200	0.582	28.012	0.094			0.288	16.719
300	0.832	30.857	0.103			0.306	16.716
400	1.053	33.265	0.111			0.323	16.713
500	1.251	36.110	0.121			0.345	16.710
		38.736	0.130			0.364	16.605
		41.581	0.139			0.386	16.703
		43.988	0.147			0.408	16.901
		46.834	0.157			0.426	16.797
		53.399	0.179			0.450	16.692
		59.964	0.200				
		66.748	0.223				
		73.313	0.245				
		80.098	0.268				
		86.663	0.290				
		93.447	0.312				
		100.231	0.335				

Table S16: Tabulated data for Figure S5: Comparison of GCMC simulations using the ITQ-29 crystal structure, and an average unit cell structure obtained from MD simulations at the temperature with experimental data from calorimetric experiments obtained during this study.

	195 K - Crystal Structure	**195 K - Avg. MD Structure**	**195 K - Exp. 1**		**195 K - Exp. 2**	
Pressure (kPa)	Loading (mol/kg)	Loading (mol/kg)	Pressure (kPa)	Loading (mol/kg)	Pressure (kPa)	Loading (mol/kg)
0.001	0.001	0.001	0.02	0.047	0.01	0.022
0.002	0.002	0.003	0.14	0.267	0.02	0.044
0.005	0.005	0.007	0.41	0.634	0.05	0.115
0.01	0.009	0.014	0.62	1.012	0.09	0.188
0.02	0.019	0.029	0.79	1.400	0.14	0.260
0.05	0.047	0.070	0.91	1.795	0.29	0.474
0.1	0.094	0.137	1.01	2.193	0.41	0.639
0.2	0.191	0.269	1.09	2.592	0.52	0.809
0.5	0.507	0.661	1.46	4.175	0.62	0.984
1	1.256	1.584	2.83	5.522	0.70	1.162
2	5.111	5.183	7.74	6.188	0.78	1.342
5	6.127	6.233	14.66	6.472	0.84	1.524
10	6.419	6.558	26.11	6.694	0.89	1.708
20	6.634	6.798	38.01	6.829	0.94	1.894
50	6.867	7.056	50.07	6.930	0.97	2.080
100	7.023	7.216	62.24	7.008	1.01	2.266
200	7.100	7.315	74.49	7.070	1.04	2.452
500	7.115	7.333	86.77	7.127	1.11	2.826
1,000	7.101	7.347	96.80	7.161	1.18	3.198
2,000	7.106	7.354	101.26	7.197	1.25	3.567
5,000	7.162	7.357			1.34	3.931
10,000	7.147	7.365			1.45	4.288
					1.60	4.634
					1.83	4.964
					2.21	5.268
					2.79	5.535
					3.64	5.756
					4.75	5.933
					6.08	6.072
					7.57	6.181
					9.17	6.270
					10.86	6.344
					22.00	6.606
					33.77	6.744

Table S17: Tabulated data for Figure S6: Heats of adsorption and loadings of CO_2 in LTA-4A from GCMC simulations and Clausius-Clapeyron analysis.

	440 K		450 K		460 K	
Pressure (kPa)	Q_{st} (kJ/mol)	Loading (mol/kg)	Q_{st} (kJ/mol)	Loading (mol/kg)	Q_{st} (kJ/mol)	Loading (mol/kg)
0.001	29.4 ± 25.8	1.10E-05 ± 1.14 E-05	44.9 ± 34.9	1.54E-05 ± 1.50E-05	38.7 ± 54.8	1.03E-05 ± 8.55E-06
0.002	37.2 ± 19.7	2.35E-05 ± 1.89E-05	44.0 ± 32.7	2.71E-05 ± 1.89E-05	54.2 ± 86.9	1.25E-05 ± 1.28E-05
0.005	47.7 ± 17.6	8.07E-05 ± 2.45E-05	41.7 ± 18.9	5.21E-05 ± 2.76E-05	36.4 ± 34.1	4.62E-05 ± 1.95E-05
0.01	41.3 ± 18.4	1.36E-04 ± 3.86E-05	37.8 ± 12.6	1.07E-04 ± 5.21E-05	42.8 ± 9.80	1.10E-04 ± 3.31E-05
0.02	44.0 ± 6.39	2.95E-04 ± 8.34E-05	43.7 ± 4.87	2.30E-04 ± 2.57E-05	46.3 ± 9.57	1.66E-04 ± 3.49E-05
0.05	43.2 ± 4.36	0.001 ± 5.31E-05	43.7 ± 7.14	0.001 ± 6.08E-05	38.2 ± 4.20	4.56E-04 ± 1.04E-04
0.1	42.1 ± 4.65	0.002 ± 1.66E-04	43.8 ± 2.64	0.001 ± 8.30E-05	42.6 ± 5.59	0.001 ± 1.22E-04
0.2	42.9 ± 4.26	0.003 ± 1.57E-04	42.8 ± 2.52	0.002 ± 2.16E-04	41.6 ± 5.62	0.002 ± 1.55E-04
0.5	43.2 ± 2.77	0.008 ± 2.80E-04	42.5 ± 2.04	0.006 ± 3.24E-04	42.0 ± 2.87	0.005 ± 2.17E-04
1	43.4 ± 1.02	0.015 ± 0.001	42.3 ± 1.57	0.011 ± 3.10E-04	43.0 ± 1.70	0.009 ± 3.07E-04
2	43.1 ± 0.69	0.031 ± 0.001	42.4 ± 2.47	0.023 ± 6.13E-04	42.8 ± 1.82	0.018 ± 0.001
5	43.0 ± 1.96	0.076 ± 0.002	43.1 ± 1.79	0.057 ± 2.72E-04	42.1 ± 1.32	0.046 ± 0.002
10	43.5 ± 1.17	0.150 ± 0.004	43.1 ± 1.08	0.113 ± 0.003	42.1 ± 1.13	0.090 ± 0.003
20	43.2 ± 0.56	0.285 ± 0.009	42.8 ± 1.07	0.225 ± 0.007	42.7 ± 1.03	0.179 ± 0.007
50	43.9 ± 0.69	0.660 ± 0.012	42.9 ± 0.92	0.520 ± 0.006	42.8 ± 0.79	0.426 ± 0.012
100	43.9 ± 0.26	1.171 ± 0.018	42.9 ± 1.02	0.936 ± 0.021	42.7 ± 1.41	0.766 ± 0.021
200	44.1 ± 1.24	1.846 ± 0.027	43.7 ± 0.83	1.547 ± 0.020	43.3 ± 0.71	1.330 ± 0.031
500	43.9 ± 1.24	2.754 ± 0.025	43.7 ± 0.47	2.485 ± 0.024	44.0 ± 0.84	2.257 ± 0.024
1,000	42.3 ± 2.17	3.289 ± 0.013	42.7 ± 0.68	3.086 ± 0.017	43.7 ± 1.10	2.912 ± 0.024
2,000	40.4 ± 1.39	3.754 ± 0.013	40.8 ± 1.06	3.594 ± 0.023	41.8 ± 1.24	3.444 ± 0.018
5,000	38.4 ± 1.33	4.282 ± 0.019	38.6 ± 1.97	4.129 ± 0.029	39.0 ± 0.40	4.022 ± 0.015
10,000	37.5 ± 1.45	4.637 ± 0.032	37.4 ± 1.44	4.490 ± 0.040	38.0 ± 1.59	4.382 ± 0.023

Clausius-Clapeyron

Loading (mol/kg)	Q_{st} (kJ/mol)
0.100	44.536
0.324	44.349
0.547	44.318
0.771	44.122
0.995	44.007
1.218	43.543
1.442	44.307
1.666	44.457
1.889	43.695
2.113	42.557
2.337	41.321
2.561	41.393
2.784	42.342
3.008	40.925
3.232	40.481

3.455	40.138
3.679	40.432
3.903	41.068
4.126	38.644
4.350	41.493

Table S18: Tabulated data for Figure S7: Heats of adsorption and loadings of CO_2 in LTA-4A from GCMC simulations and Clausius-Clapeyron analysis.

	570 K		600 K		630 K	
Pressure (kPa)	Q_{st} (kJ/mol)	Loading (mol/kg)	Q_{st} (kJ/mol)	Loading (mol/kg)	Q_{st} (kJ/mol)	Loading (mol/kg)
0.001	----	7.33E-07 ± 2.93E-06	----	----	----	----
0.002	----	2.93E-06 ± 5.49E-06	----	7.33E-07 ± 2.93E-06	----	1.47E-06 ± 5.87E-06
0.005	----	7.33E-06 ± 9.28E-06	----	4.40E-06 ± 5.49E-06	----	1.47E-06 ± 3.59E-06
0.01	19.0 ± 47.6	1.61E-05 ± 2.20E-05	32.5 ± 41.1	1.10E-06 ± 1.14E-06	----	5.13E-06 ± 7.48E-06
0.02	43.2 ± 35.0	3.37E-05 ± 1.42E-05	40.4 ± 53.5	2.05E-05 ± 7.48E-06	----	1.39E-05 ± 1.88E-05
0.05	35.2 ± 12.1	5.28E-05 ± 3.92E-05	40.3 ± 43.4	3.89E-05 ± 2.39E-05	20.2 ± 44.3	3.15E-05 ± 1.10E-05
0.1	37.2 ± 5.25	1.14E-04 ± 1.82E-05	16.4 ± 18.2	8.51E-05 ± 1.57E-05	30.4 ± 34.1	6.75E-05 ± 1.77E-05
0.2	38.1 ± 11.9	2.70E-04 ± 4.63E-05	34.1 ± 10.3	1.72E-04 ± 1.99E-05	49.2 ± 20.5	1.15E-04 ± 3.33E-05
0.5	42.4 ± 4.28	0.001 ± 9.98E-05	41.2 ± 7.58	4.58E-04 ± 6.85E-05	34.3 ± 6.56	2.87E-04 ± 6.45E-05
1	38.6 ± 3.93	0.001 ± 8.51E-05	40.4 ± 9.64	8.63E-04 ± 2.30E-05	37.7 ± 7.33	0.001 ± 7.56E-05
2	38.5 ± 3.62	0.002 ± 7.00E-05	37.5 ± 7.26	0.002 ± 1.91E-04	36.3 ± 4.96	0.001 ± 9.49E-05
5	38.5 ± 1.29	0.006 ± 3.34E-04	35.7 ± 5.24	0.004 ± 3.01E-04	36.2 ± 5.26	0.003 ± 1.10E-04
10	38.7 ± 0.63	0.012 ± 4.52E-04	37.6 ± 3.33	0.008 ± 2.79E-04	37.6 ± 3.74	0.006 ± 3.85E-04
20	38.4 ± 1.85	0.024 ± 0.001	37.7 ± 1.11	0.017 ± 4.58E-04	36.7 ± 2.44	0.012 ± 3.01E-04
50	38.3 ± 1.30	0.061 ± 0.001	37.6 ± 0.70	0.042 ± 3.87E-04	36.4 ± 1.47	0.029 ± 0.001
100	38.8 ± 0.48	0.120 ± 0.004	37.9 ± 1.63	0.083 ± 0.002	37.3 ± 1.37	0.058 ± 0.001
200	38.7 ± 1.01	0.232 ± 0.002	38.2 ± 1.34	0.162 ± 0.003	37.0 ± 1.49	0.115 ± 0.002
500	39.3 ± 0.73	0.538 ± 0.009	38.2 ± 0.87	0.38 ± 0.006	36.9 ± 0.59	0.277 ± 0.004
1,000	39.4 ± 0.40	0.946 ± 0.009	38.0 ± 1.22	0.694 ± 0.014	37.5 ± 0.73	0.516 ± 0.011
2,000	40.1 ± 0.55	1.548 ± 0.021	39.3 ± 0.79	1.183 ± 0.025	37.9 ± 0.85	0.912 ± 0.010
5,000	40.8 ± 0.81	2.449 ± 0.016	39.7 ± 0.90	2.041 ± 0.021	38.9 ± 1.02	1.681 ± 0.006
10,000	40.7 ± 0.74	3.083 ± 0.032	40.2 ± 0.71	2.715 ± 0.015	39.3 ± 1.36	2.362 ± 0.018

Clausius-Clapeyron

Loading (mol/kg)	Q_{st} (kJ/mol)
0.100	36.502
0.344	36.461
0.589	36.905
0.833	36.692
1.078	37.470
1.322	38.495
1.567	38.691
1.811	38.553
2.056	38.986
2.300	38.878

Table S19: Tabulated data for Figure S8: Heats of adsorption and loadings of CO_2 in ITQ-29 from GCMC simulations and Clausius-Clapeyron analysis.

	190 K		195 K		200 K	
Pressure (kPa)	Q_{st} (kJ/mol)	Loading (mol/kg)	Q_{st} (kJ/mol)	Loading (mol/kg)	Q_{st} (kJ/mol)	Loading (mol/kg)
0.001	27.8 ± 0.21	0.002 ± 1.29E-04	27.4 ± 0.44	0.002 ± 1.66E-04	27.5 ± 0.28	0.001 ± 9.38E-05
0.002	27.7 ± 0.25	0.005 ± 4.22E-04	27.5 ± 0.22	0.003 ± 4.14E-04	27.2 ± 0.39	0.002 ± 1.85E-04
0.005	27.8 ± 0.21	0.012 ± 0.001	27.4 ± 0.17	0.008 ± 0.001	27.0 ± 0.29	0.005 ± 4.35E-04
0.01	27.7 ± 0.36	0.024 ± 0.003	27.6 ± 0.19	0.016 ± 0.002	27.3 ± 0.21	0.010 ± 0.001
0.02	27.6 ± 0.14	0.048 ± 0.003	27.4 ± 0.14	0.031 ± 0.003	27.3 ± 0.34	0.021 ± 0.002
0.05	27.4 ± 0.40	0.121 ± 0.014	27.4 ± 0.34	0.078 ± 0.006	27.1 ± 0.21	0.049 ± 0.003
0.1	27.1 ± 0.18	0.221 ± 0.024	27.1 ± 0.25	0.153 ± 0.009	27.0 ± 0.12	0.101 ± 0.009
0.2	26.7 ± 0.38	0.463 ± 0.036	26.7 ± 0.45	0.299 ± 0.014	26.6 ± 0.20	0.192 ± 0.007
0.5	25.4 ± 0.72	1.223 ± 0.125	25.8 ± 0.21	0.776 ± 0.065	26.0 ± 0.43	0.497 ± 0.031
1	28.3 ± 0.35	4.890 ± 0.060	25.8 ± 0.27	1.997 ± 0.168	25.1 ± 0.10	1.057 ± 0.061
2	31.0 ± 0.70	6.008 ± 0.051	29.3 ± 0.52	5.411 ± 0.066	27.2 ± 0.31	3.962 ± 0.089
5	31.5 ± 0.65	6.474 ± 0.032	31.2 ± 1.03	6.249 ± 0.045	30.8 ± 0.64	5.954 ± 0.047
10	31.4 ± 2.16	6.718 ± 0.038	31.0 ± 1.25	6.555 ± 0.030	31.3 ± 1.21	6.360 ± 0.055
20	31.4 ± 1.62	6.908 ± 0.060	31.6 ± 1.06	6.758 ± 0.052	31.1 ± 0.51	6.625 ± 0.032
50	31.0 ± 1.10	7.107 ± 0.093	30.6 ± 2.50	6.989 ± 0.072	31.0 ± 2.59	6.887 ± 0.074
100	30.7 ± 2.43	7.262 ± 0.017	30.8 ± 1.39	7.192 ± 0.056	31.1 ± 1.80	7.037 ± 0.106
200	30.4 ± 2.31	7.283 ± 0.041	29.3 ± 1.55	7.287 ± 0.098	30.0 ± 1.78	7.231 ± 0.135
500	29.7 ± 3.97	7.325 ± 0.029	30.2 ± 2.41	7.309 ± 0.063	30.1 ± 4.24	7.249 ± 0.084
1,000	30.5 ± 1.97	7.357 ± 0.093	29.2 ± 2.54	7.268 ± 0.125	30.5 ± 4.63	7.253 ± 0.115
2,000	30.0 ± 3.07	7.350 ± 0.079	29.4 ± 3.16	7.318 ± 0.047	30.7 ± 1.62	7.238 ± 0.076
5,000	30.1 ± 3.09	7.371 ± 0.096	29.5 ± 2.36	7.319 ± 0.091	29.5 ± 4.03	7.206 ± 0.159
10,000	29.5 ± 5.39	7.355 ± 0.103	30.2 ± 2.71	7.340 ± 0.062	29.1 ± 1.90	7.284 ± 0.035

Clausius-Clapeyron

Loading (mol/kg)	Q_{st} (kJ/mol)
0.002	27.390
0.004	27.008
0.007	26.709
0.012	26.437
0.021	26.853
0.035	27.423
0.060	26.882
0.102	27.116
0.174	26.592
0.296	26.718
0.504	26.400
0.860	25.196

0.774	25.503
1.111	25.318
1.447	25.323
1.784	25.655
2.121	25.778
2.458	25.859
2.795	26.074
3.132	26.403
3.468	26.829
3.805	27.331
4.142	27.878
4.479	28.429
4.816	28.955
5.153	29.424
5.489	29.501

Table S20: Tabulated data for Figure S9: Heats of adsorption of CH_4 in ITQ-29 at 195 K calculated by different methods (GCMC fluctuation formula, Clausius-Clapeyron equation).

GCMC Fluctuations		Clausius-Clapeyron	
Loading (mol/kg)	Q_{st} (kJ/mol)	Loading (mol/kg)	Q_{st} (kJ/mol)
5.37E-05	13.4	0.022	13.1
9.88E-05	13.5	0.370	13.5
2.70E-04	13.6	0.719	14.1
0.001	13.5	1.067	14.5
0.001	13.6	1.415	14.7
0.003	13.5	1.764	15.1
0.005	13.5	2.112	15.4
0.011	13.5	2.460	15.1
0.027	13.6	2.808	16.4
0.053	13.6	3.157	16.0
0.108	13.7	3.505	16.6
0.273	13.8	3.853	15.6
0.558	14.1	4.202	16.0
1.114	14.7	4.550	16.1
2.310	15.7	4.898	16.1
3.265	16.6	5.246	17.2
3.970	17.1		
4.710	17.4		
5.174	17.4		
5.693	17.9		
6.260	18.2		
6.530	18.2		

Table S21: Tabulated data for Figure S10: CO_2 positions in LTA-4A.

300 K						450 K					
% of CO_2 molecules in dual cation sites	Counts	% of CO_2 molecules in single cation sites	Counts	% of CO_2 molecules with O-Na distances > 3.5 Å	Counts	% of CO_2 molecules in dual cation sites	Counts	% of CO_2 molecules in single cation sites	Counts	% of CO_2 molecules with O-Na distances > 3.5 Å	Counts
0	1	0	710	0	9023	0	6	0	153	0	6761
5	0	5	191	5	268	5	0	5	64	5	1259
10	0	10	1137	10	562	10	1	10	400	10	1388
15	0	15	1594	15	125	15	6	15	769	15	446
20	1	20	1781	20	18	20	14	20	1190	20	111
25	5	25	1473	25	1	25	21	25	1409	25	26
30	4	30	933	30	2	30	37	30	1254	30	8
35	20	35	955	35	1	35	113	35	1508	35	0
40	38	40	558	40	0	40	244	40	1268	40	1
45	95	45	338	45	0	45	460	45	912	45	0
50	217	50	189	50	0	50	613	50	464	50	0
55	364	55	80	55	0	55	1175	55	323	55	0
60	447	60	26	60	0	60	1152	60	137	60	0
65	1191	65	29	65	0	65	1825	65	98	65	0
70	994	70	2	70	0	70	1224	70	22	70	0
75	1528	75	3	75	0	75	1293	75	16	75	0
80	1761	80	0	80	0	80	879	80	7	80	0
85	1189	85	0	85	0	85	440	85	2	85	0
90	1360	90	0	90	0	90	354	90	0	90	0
95	161	95	0	95	0	95	31	95	0	95	0
100	624	100	1	100	0	100	112	100	4	100	0

600 K					
% of CO_2 molecules in dual cation sites	Counts	% of CO_2 molecules in single cation sites	Counts	% of CO_2 molecules with O-Na distances > 3.5 Å	Counts
0	48	0	213	0	5372
5	0	5	4	5	348
10	28	10	171	10	1990
15	120	15	518	15	1286
20	163	20	642	20	583
25	227	25	759	25	193
30	252	30	810	30	94
35	601	35	1226	35	85

40	867	40	1267	40	25
45	1108	45	1189	45	12
50	1321	50	1091	50	10
55	1288	55	798	55	1
60	818	60	383	60	0
65	1329	65	516	65	1
70	527	70	129	70	0
75	514	75	108	75	0
80	340	80	77	80	0
85	215	85	51	85	0
90	133	90	21	90	0
95	1	95	0	95	0
100	100	100	27	100	0

Table S22: Tabulated data for Figure S11: Interaction energies of CO_2 in different sites in LTA-4A.

No Cation		Single Cation		Dual Cation	
Interaction Energy / CO_2 molecule (kJ/mol)	Counts	Interaction Energy / CO_2 molecule (kJ/mol)	Counts	Interaction Energy / CO_2 molecule (kJ/mol)	Counts
-63	0	-63	1	-63	0
-61	2	-61	0	-61	10
-59	1	-59	3	-59	27
-57	11	-57	12	-57	76
-55	9	-55	31	-55	214
-53	34	-53	104	-53	529
-51	57	-51	258	-51	821
-49	71	-49	585	-49	758
-47	135	-47	838	-47	448
-45	147	-45	766	-45	231
-43	172	-43	439	-43	101
-41	142	-41	240	-41	43
-39	125	-39	103	-39	19
-37	95	-37	33	-37	6
-35	89	-35	18	-35	2
-33	63	-33	6	-33	1
-31	45	-31	1		
-29	36	-29	0		
-27	25	-27	2		
-25	13	-25	2		
-23	14				
-21	4				
-19	2				
-17	4				
-15	1				
-13	0				
-11	1				

Table S23: Tabulated data for Figure S12: CO_2 positions in Na-LTA Si/Al = 2.

303 K						453 K					
% of CO_2 molecules in dual cation sites	Counts	% of CO_2 molecules in single cation sites	Counts	% of CO_2 molecules with O-Na distances > 3.5 Å	Counts	% of CO_2 molecules in dual cation sites	Counts	% of CO_2 molecules in single cation sites	Counts	% of CO_2 molecules with O-Na distances > 3.5 Å	Counts
0	92	0	4629	0	43	0	95	0	672	0	41
5	0	5	231	5	0	5	10	5	160	5	3
10	16	10	2032	10	9	10	137	10	1183	10	97
15	255	15	1579	15	95	15	367	15	1455	15	260
20	327	20	795	20	149	20	630	20	1730	20	553
25	468	25	330	25	249	25	897	25	1481	25	904
30	610	30	167	30	350	30	1011	30	1009	30	1030
35	1257	35	126	35	851	35	1455	35	927	35	1536
40	1570	40	59	40	1313	40	1644	40	659	40	1731
45	1526	45	17	45	1601	45	1485	45	376	45	1557
50	1543	50	29	50	1887	50	927	50	183	50	954
55	1012	55	2	55	1263	55	676	55	78	55	645
60	486	60	0	60	641	60	261	60	37	60	282
65	523	65	4	65	913	65	274	65	27	65	252
70	124	70	0	70	246	70	59	70	12	70	64
75	98	75	0	75	173	75	39	75	4	75	43
80	45	80	0	80	104	80	20	80	5	80	29
85	25	85	0	85	69	85	7	85	1	85	10
90	2	90	0	90	8	90	2	90	0	90	1
95	0	95	0	95	0	95	1	95	0	95	0
100	21	100	0	100	36	100	3	100	1	100	8

600K					
% of CO_2 molecules in dual cation sites	Counts	% of CO_2 molecules in single cation sites	Counts	% of CO_2 molecules with O-Na distances > 3.5 Å	Counts
0	497	0	355	0	297
5	13	5	5	5	9
10	490	10	287	10	321
15	1012	15	652	15	755
20	1214	20	923	20	1046
25	1187	25	910	25	1074
30	1042	30	917	30	1040
35	1343	35	1315	35	1370

40	1093	40	1221	40	1265
45	813	45	1053	45	988
50	590	50	870	50	819
55	298	55	590	55	412
60	129	60	286	60	198
65	177	65	341	65	248
70	35	70	89	70	47
75	30	75	74	75	50
80	14	80	50	80	32
85	13	85	32	85	16
90	2	90	11	90	3
95	0	95	0	95	0
100	8	100	19	100	10

Table S24: Tabulated data for Figure S13: CO_2 positions in ITQ-29.

300 K						450 K					
% of CO_2 molecules in 6MR	Counts	% of CO_2 molecules in 8MR	Counts	% of CO_2 molecules in 4MR	Counts	% of CO_2 molecules in 6MR	Counts	% of CO_2 molecules in 8MR	Counts	% of CO_2 molecules in 4MR	Counts
0	172	0	1753	0	8458	0	31	0	1793	0	7568
5	6	5	397	5	409	5	7	5	1148	5	1097
10	136	10	1751	10	775	10	109	10	2330	10	1011
15	417	15	2084	15	272	15	245	15	2114	15	250
20	635	20	1590	20	61	20	460	20	1412	20	52
25	872	25	1051	25	14	25	827	25	715	25	15
30	848	30	499	30	6	30	967	30	267	30	6
35	1346	35	423	35	2	35	1375	35	128	35	0
40	1405	40	227	40	0	40	1586	40	67	40	1
45	1283	45	109	45	0	45	1627	45	18	45	0
50	1015	50	82	50	2	50	937	50	5	50	0
55	734	55	11	55	0	55	901	55	2	55	0
60	375	60	10	60	0	60	383	60	0	60	0
65	412	65	5	65	0	65	351	65	1	65	0
70	130	70	0	70	0	70	105	70	0	70	0
75	92	75	1	75	0	75	52	75	0	75	0
80	63	80	1	80	0	80	17	80	0	80	0
85	30	85	0	85	0	85	10	85	0	85	0
90	8	90	0	90	0	90	10	90	0	90	0
95	0	95	0	95	0	95	0	95	0	95	0
100	21	100	6	100	1	100	0	100	0	100	0

600 K					
% of CO_2 molecules in 6MR	Counts	% of CO_2 molecules in 8MR	Counts	% of CO_2 molecules in 4MR	Counts
0	173	0	3378	0	8169
5	2	5	263	5	172
10	161	10	2188	10	1029
15	427	15	1799	15	468
20	650	20	1154	20	111
25	754	25	531	25	27
30	787	30	273	30	5
35	1211	35	222	35	15
40	1354	40	117	40	3
45	1248	45	35	45	0
50	1107	50	28	50	1
55	790	55	4	55	0
60	403	60	4	60	0

65	495	65	3	65	0
70	157	70	0	70	0
75	126	75	0	75	0
80	84	80	0	80	0
85	41	85	0	85	0
90	9	90	0	90	0
95	0	95	0	95	0
100	21	100	1	100	0

Table S25: Tabulated data for Figure S14: CO_2 positions in Si-CHA.

300 K						450 K					
% of CO_2 molecules in 6MR	Counts	% of CO_2 molecules in 8MR	Counts	% of CO_2 molecules in 4MR	Counts	% of CO_2 molecules in 6MR	Counts	% of CO_2 molecules in 8MR	Counts	% of CO_2 molecules in 4MR	Counts
0	0	0	0	0	367	0	2	0	0	0	328
5	27	5	0	5	126	5	31	5	0	5	163
10	90	10	0	10	8	10	95	10	0	10	10
15	187	15	0	15	0	15	150	15	0	15	0
20	139	20	0	20	0	20	130	20	0	20	0
25	51	25	0	25	0	25	73	25	0	25	0
30	7	30	0	30	0	30	18	30	0	30	0
35	0	35	0	35	0	35	2	35	3	35	0
40	0	40	0	40	0	40	0	40	12	40	0
45	0	45	8	45	0	45	0	45	34	45	0
50	0	50	31	50	0	50	0	50	72	50	0
55	0	55	84	55	0	55	0	55	115	55	0
60	0	60	119	60	0	60	0	60	105	60	0
65	0	65	143	65	0	65	0	65	84	65	0
70	0	70	73	70	0	70	0	70	55	70	0
75	0	75	40	75	0	75	0	75	19	75	0
80	0	80	3	80	0	80	0	80	2	80	0
85	0	85	0	85	0	85	0	85	0	85	0
90	0	90	0	90	0	90	0	90	0	90	0
95	0	95	0	95	0	95	0	95	0	95	0
100	0	100	0	100	0	100	0	100	0	100	0

600 K					
% of CO_2 molecules in 6MR	Counts	% of CO_2 molecules in 8MR	Counts	% of CO_2 molecules in 4MR	Counts
0	1	0	0	0	317
5	43	5	0	5	178
10	107	10	0	10	6
15	166	15	0	15	0
20	108	20	0	20	0
25	55	25	0	25	0
30	17	30	1	30	0
35	3	35	3	35	0
40	1	40	13	40	0
45	0	45	41	45	0
50	0	50	80	50	0
55	0	55	94	55	0
60	0	60	109	60	0

65	0	65	86	65	0
70	0	70	45	70	0
75	0	75	18	75	0
80	0	80	11	80	0
85	0	85	0	85	0
90	0	90	0	90	0
95	0	95	0	95	0
100	0	100	0	100	0

References:

1. Fang, H.; Kamakoti, P.; Ravikovitch, P. I.; Aronson, M.; Paur, C.; Sholl, D. S. "First Principles Derived, Transferable Force Fields for CO_2 Adsorption in Na-Exchanged Cationic Zeolites." *Phys. Chem. Chem. Phys.* **2013,** *15* (31), 12882-12894.
2. Akten, E. D.; Siriwardane, R.; Sholl, D. S. "Monte Carlo Simulation of Single- and Binary-Component Adsorption of CO_2, N_2, and H_2 in Zeolite Na-4A." *Energy Fuels* **2003,** *17* (4), 977-983.
3. Jaramillo, E.; Chandross, M. "Adsorption of Small Molecules in LTA Zeolites. 1. NH_3, CO_2, and H_2O in Zeolite 4A." *J. Phys. Chem. B* **2004,** *108* (52), 20155-20159.
4. Maurin, G.; Llewellyn, P. L.; Bell, R. G. "Adsorption Mechanism of Carbon Dioxide in Faujasites: Grand Canonical Monte Carlo Simulations and Microcalorimetry Measurements." *J. Phys. Chem. B* **2005,** *109* (33), 16084-16091.
5. García-Pérez, E.; Parra, J. B.; Ania, C. O.; García-Sánchez, A.; van Baten, J. M.; Krishna, R.; Dubbeldam, D.; Calero, S. "A Computational Study of CO_2, N_2, and CH_4 Adsorption in Zeolites." *Adsorption* **2007,** *13* (5-6), 469-476.
6. García-Sánchez, A.; Ania, C. O.; Parra, J. B.; Dubbeldam, D.; Vlugt, T. J. H.; Krishna, R.; Calero, S. "Transferable Force Field for Carbon Dioxide Adsorption in Zeolites." *J. Phys. Chem. C* **2009,** *113* (20), 8814-8820.
7. Pham, T. D.; Xiong, R.; Sandler, S. I.; Lobo, R. F. "Experimental and Computational Studies on the Adsorption of CO_2 and N_2 on Pure Silica Zeolites." *Microporous Mesoporous Mater.* **2014,** *185* (1 February 2014), 157-166.
8. Vujić, B.; Lyubartsev, A. P. "Transferable Force-Field for Modelling of CO_2, N_2, O_2 and Ar in All Silica and Na^+ Exchanged Zeolites." *Modell. Simul. Mater. Sci. Eng.* **2016,** *24*, 045002(1-26).
9. Cygan, R. T.; Liang, J.-J.; Kalinichev, A. G. "Molecular Models of Hydroxide, Oxyhydroxide, and Clay Phases and the Development of a General Force Field." *J. Phys. Chem. B* **2004,** *108* (4), 1255-1266.
10. Bai, P.; Tsapatsis, M.; Siepmann, J. I. "TraPPE-zeo: Transferable Potentials for Phase Equilibria Force Field for All-Silica Zeolites." *J. Phys. Chem. C* **2013,** *117* (46), 24375-24387.
11. Talu, O.; Myers, A. L. "Reference Potentials for Adsorption of Helium, Argon, Methane, and Krypton in High-Silica Zeolites." *Colloids Surf., A* **2001,** *187-188* (31 August 2001), 83-93.
12. Harris, J. G.; Yung, K. H. "Carbon Dioxide's Liquid-Vapor Coexistence Curve and Critical Properties As Predicted by a Simple Molecular Model." *J. Phys. Chem.* **1995,** *99* (31), 12021-12024.
13. Potoff, J. J.; Siepmann, J. I. "Vapor–Liquid Equilibria of Mixtures Containing Alkanes, Carbon Dioxide, and Nitrogen." *AIChE J.* **2001,** *47* (7), 1676-1682.
14. Fang, H.; Awati, R. V.; Boulfelfel, S. E.; Ravikovitch, P. I.; Sholl, D. S. "First-Principles-Derived Force Fields for CH4 Adsorption and Diffusion in Siliceous Zeolites." *J. Phys. Chem. C* **2018,** *122* (24), 12880-12891.
15. Bludský, O.; Rubeš, M.; Soldán, P.; Nachtigall, P. "Invesitgation of the Benzene-Dimer Potential Energy Surface: DFT/CCSD(T) Correction Scheme." *J. Chem. Phys.* **2008,** *128* (11), 114102.
16. Otero Areán, C.; Turnes Palomino, G.; Llop Carayol, M. R.; Pulido, A.; Rubeš, M.; Bludský, O.; Nachtigall, P. "Hydrogen adsorption on the zeolite Ca-A: DFT and FT-IR investigation." *Chem. Phys. Lett.* **2009,** *477* (1-3), 139-143.
17. Martin, M. G.; Siepmann, J. I. "Transferable Potentials for Phase Equilibria. 1. United-Atom Description of *n*-Alkanes." *J. Phys. Chem. B* **1998,** *102* (14), 2569-2577.

18. Manz, T. A.; Sholl, D. S. "Improved Atoms-in-Molecule Charge Partitioning Functional for Simultaneously Reproducing the Electrostatic Potential and Chemical States in Periodic and Nonperiodic Materials." *J. Chem. Theory Comput.* **2012,** *8* (8), 2844-2867.
19. Manz, T. A.; Sholl, D. S. "Methods for Computing Accurate Atomic Spin Moments for Collinear and Noncollinear Magnetism in Periodic and Nonperiodic Materials." *J. Chem. Theory Comput.* **2011,** *7* (12), 4146.
20. Manz, T. A.; Sholl, D. S. "Chemically Meaningful Atomic Charges that Reproduce the Electrostatic Potential in Periodic and Nonperiodic Materials." *J. Chem. Theory Comput.* **2010,** *6* (8), 2455-2468.
21. Harper, R. J.; Stifel, G. R.; Anderson, R. B. "Adsorption of gases on 4A synthetic zeolite." *Can. J. Chem.* **1969,** *47* (24), 4661-4670.
22. Li, Y.; Yi, H.; Tang, X.; Li, F.; Yuan, Q. "Adsorption separation of CO_2/CH_4 gas mixture on the commercial zeolites at atmospheric pressure." *Chem. Eng. J (Amsterdam, Neth.)* **2013,** *229*, 50-56.
23. Ahmed, M. J.; Theydan, S. K. "Equilibrium isotherms studies for light hydrocarbons adsorption on 4A molecular sieve zeolite." *J. Pet. Sci. Eng.* **2013,** *108*, 316-320.
24. Eagan, J. D.; Anderson, R. B. "Kinetics and Equilibrium of Adsorption on 4A Zeolite." *J. Colloid Interface Sci.* **1975,** *50* (3), 419-433.
25. Jensen, N. K.; Rufford, T. E.; Watson, G.; Zhang, D. K.; Chan, K. I.; May, E. F. "Screening Zeolites for Gas Separation Applications Involving Methane, Nitrogen, and Carbon Dioxide." *J. Chem. Eng. Data* **2012,** *57* (1), 106-113.
26. Palomino, M.; Corma, A.; Rey, F.; Valencia, S. "New Insights on CO_2−Methane Separation Using LTA Zeolites with Different Si/Al Ratios and a First Comparison with MOFs." *Langmuir* **2010,** *26* (3), 1910-1917.
27. Pluth, J. J.; Smith, J. V. "Accurate Redetermination of Crystal Structure of Dehydrated Zeolite A. Absence of Near Zero Coordination of Sodium. Refinement of Si,Al-Ordered Superstructure." *J. Am. Chem. Soc.* **1980,** *102* (14), 4704-4708.
28. Vlugt, T. J. H.; García-Pérez, E.; Dubbeldam, D.; Ban, S.; Calero, S. "Computing the Heat of Adsorption using Molecular Simulations: The Effect of Strong Coulombic Interactions." *J. Chem. Theory Comput.* **2008,** *4*, 1107-1118.
29. Plimpton, S. "Fast Parallel Algorithms for Short-Range Molecular Dynamics." *J. Comput. Phys.* **1995,** *117* (1), 1-19.
30. Awati, R. "Development of Accurate Computational Methods for Simulations of Adsorption and Diffusion in Zeolites." Ph.D. Thesis, Georgia Institute of Technology, May 2016.
31. Corma, A.; Rey, F.; Rius, J.; Sabater, M. J.; Valencia, S. "Supramolecular Self-Assembled Molecules as Organic Directing Agent for Synthesis of Zeolites." Nature 2004, 431, 287-290.